Titanium Dioxide Nanotubes Reinforced Bone Cement Composite:

Cytotoxicity And Mechanical Properties

BY

ABHIJIT HARIBHAU PHAKATKAR B. Tech., University of Pune, India, 2012

THESIS

Submitted as partial fulfillment of the requirements for the degree of Master of Science in Mechanical Engineering in the Graduate College of the University of Illinois at Chicago, 2018

Chicago, Illinois

Defense Committee:

Tolou Shokuhfar, Chair and Advisor, Bioengineering Reza Shahbazian-Yassar, Co-advisor, Mechanical and Industrial Engineering Mathew Mathew, Bioengineering Megha Agrawal, Bioengineering This thesis is dedicated to my Mother (Bharati) whose caring and loving heart has always provided me strength for my life endeavors and my Father (Dr. Haribhau G. Phakatkar, Prof. Mechanical Engineering and Principal) whose timely support helps me to rise above difficult circumstances and achieve success. Also, I would like to dedicate this work to my elder Sister (Anuprita), her caring husband (Bhupendra) and their new born cute baby (Arnav) who have always been backbone behind my every achievement. Finally, I dedicate this work to my academic advisors Dr. Tolou Shokuhfar and Dr. Reza Shahbazian-Yassar who guided me in every aspect of my life and played a pivotal role in my accomplishments for the past two years.

ACKNOWLEDGEMENTS

I would like to thank my thesis advisors Dr. Tolou Shokuhfar and Dr. Reza Shahbazian-Yassar for giving me research opportunity in biomedical and nanotechnology fields and guiding me with every single aspect of my Master's thesis project. Their support and encouragement in all the difficult situations have always provided me strength to overcome project obstacles. I am thankful to Dr. Megha Agrawal for her time and teaching me experiments from microbiology field which are very crucial to achieve my thesis project objectives, by taking into the consideration my different academic background of mechanical engineering. I appreciate the timely support provided by Dr. Issa and Dr. Khetani during my experimentation. I would also like to acknowledge the support given by Dr. Mathew Mathew on various occasions during my masters.

This acknowledgement will not be complete without mentioning the contribution of the several students from our In-Situ Nanomedicine Laboratory (ISNL) and from NanoEngineering Laboratory, UIC. I am thankful to Dr. Sweetu Patel (graduated PhD student) who taught me my first experiment in the nanotechnology field and guided me there onwards in learning variety of experiments. I will never forget the support I have been provided by Surya Narayanan (PhD student) during many difficult situations and always helping me for nanomaterials characterizations. I also thank to Meili Qi (PhD Student), who helped me with various aspects of this project along with her passionate attitude. I am grateful for the support that I received from David Banner (PhD student) for bacterial studies and Tara Foroozan (PhD student) for nanomaterials characterization. I really acknowledge the administrative support I have been provided by Dr. Emre Firlar (Post-doc researcher) for last two years. I will always remember the fun I had working with other fellow masters students in the lab Vikram, Nasim and Sai.

Finally, I would like to appreciate the backing which I always receive from all my close friends located in India, USA and Europe and my tennis coaches who have always been integral part of life.

iii

TABLE OF CONTENTS

CHAPTER

PAGE

1.	INTR	ODUCTION	.01
	1.1	Bone cements	.01
	1.2	Total hip arthroplasty (THA)	.02
	1.2.1	Femur bone in human body	.02
	1.2.2	Hip implant assembly and locations of bone cement applications	.03
	1.2.3	Reasons for revision hip surgeries – hip implants failure	06
	1.3	Total knee arthroplasty (TKA)	07
	1.4	Need for the improvisation of the state of the art bone cements	.09

2. POLYMETHYLMETHACRYLATE (PMMA) BONE CEMENT COMPOSITES.10

2.1	Overview	10
2.2	PMMA bone cement composition and polymerization process	.11
2.3	Mechanical properties of PMMA bone cements	.13
2.4	Limitations of PMMA bone cement composites	14
2.4.1	High curing temperature	14
2.4.2	Factors affecting mechanical strength of PMMA	15
2.4.3	Chemical necrosis	15
2.4.4	Lacking bioactivity	.15
2.4.5	Insufficient radiopacity	16
2.5	PMMA bone cement – bone cells interaction	.16
2.5.1	Bone extracellular matrix	16

CHAP	TER		<u>PAGE</u>
	2.5.2	Bone cells	16
	2.5.3	PMMA – MTT cells viability assay	17
	2.6	PMMA antibacterial studies	18
	2.7	Importance of TiO ₂ in biomedical field	19
3.		NANOTUBES SYNTHESIS BY RAPID BREAKDOWN DZATION (RBA) METHOD	21
	3.1	Overview	21
	3.2	Rapid breakdown anodization reaction mechanism understanding	22
	3.3	Rapid breakdown anodization process parameters	24
	3.3.1	Effect of the applied potential	24
	3.3.2	Effect of the electrolyte species	
	3.3.3	Effect of the electrolyte pH	
	3.3.4	Effect of the electrolyte temperature	26
	3.3.5	Effect of the counter electrode material	27
	3.3.6	Effect of the electrodes surface area	
	3.3.7	Effect of the magnetic stirring	29
	3.4	Understanding of rapid breakdown anodization process with corrosion aspects	29
	3.5	Overview of TiO ₂ nanotubes synthesis by electrochemical anodization process	

CHAR	PTER	I	PAGE
4.	TiO ₂	NANOTUBES SYNTHESIS BY HYDROTHERMAL METHOD	35
	4.1	Overview	35
	4.2	Hydrothermal process understanding	35
	4.2.1	Process description	36
	4.2.2	Pressure – Temperature diagram in relation with volume (filling fraction)	36
	4.2.3	Role of mineralizer (catalyst)	38
	4.2.4	Factors governing solubility of metal oxides in water	38
	4.3	Formation mechanism of hydrothermal synthesis of TiO ₂ nanotubes	40
	4.4	Hydrothermal synthesis of TiO ₂ nanotubes process control parameters	42
	4.4.1	Pretreatment – ultrasonication	42
	4.4.2	Alkali concentration	42
	4.4.3	Precursor	42
	4.4.4	Temperature	43
	4.4.5	Process time	43
	4.5	Applications of TiO ₂ nanotubes synthesized by hydrothermal method	44
5.	PROJ	IECT OBJECTIVES	45
6.	MAT	ERIALS AND METHODS	47
	6.1	Synthesis of TiO ₂ nanotubes by rapid breakdown anodization (RBA) method.	47
	6.1.1	Materials	47

<u>CHAP</u>	ΓER	<u>P</u> A	AGE
	6.1.2	Method	47
	6.2	TiO ₂ nanotubes synthesis by hydrothermal method	48
1	6.2.1	Materials	48
	6.2.2	Method	48
1	6.3	Ag-HA nanobelts synthesis by hydrothermal method	49
1	6.3.1	Materials	49
	6.3.2	Method	49
	6.4	MTT cells viability assay	50
	6.4.1	Materials	50
1	6.4.2	Method	51
1	6.5	Compression test	52
1	6.5.1	Materials	52
1	6.5.2	Method	52
1	6.6	In-vitro antibacterial test	52
1	6.6.1	Materials	52
	6.6.2	Method	53
7.	RESU	LTS AND DISCUSSION	54
	7.1	Characterization of TiO ₂ nanotubes synthesized by RBA	54
	7.2	Characterization of TiO ₂ nanotubes synthesized by hydrothermal method	55
	7.3	Characterization of Ag-HA nanobelts	57

CHAPTE	<u>ER</u>	PAGE
7.4	4 Cytotoxicity of PMMA bone cement composites by MTT assay	59
7.5	5 Compression test	62
7.6	6 In-vitro antibacterial test	64
8. CO	ONCLUSIONS	66
	UTURE SCOPE	
VI	ITA	80

LIST OF ABBREVIATIONS

ABBRIVIATION	DEFINITION
РММА	Polymethylmethacrylate
CaS	Calcium sulfate
CaP	Calcium phosphate
THA	Total hip arthroplasty
AJRR	American Joint Replacement Registry
TKA	Total knee arthroplasty
BPO	Benzoyl peroxide
ZrO_2	Zirconium dioxide
MMA	Methyl methacrylate
dMpT	N,N -dimethyl p-toluidine
ISO	International Organization for Standardization
НА	Hydroxyapatite
TiO ₂	Titanium dioxide
MWCNT	Multi-walled carbon nanotubes
MTT	3-(4,5-dimethylthiazol-2-yl)-2,5diphenyl tetrazolium bromide
DMSO	Dimethyl sulfoxide
UV	Ultraviolet
RBA	Rapid breakdown anodization
TEM	Transmission electron microscopy
FESEM	Field emission scanning electron microscopy
EDS	energy dispersive X-ray spectroscopy
XRD	X-ray diffraction

LIST OF ABBREVIATIONS (continued)

ABBRIVIATION	DEFINITION
Ag-HA	Silver doped hydroxyapatite
DI	deionized
Ti	Titanium
PBS	Phosphate buffer saline
Penstrep	Penicillin streptomycin

LIST OF TABLES

TABLE	PAGE
TABLE 01 – PMMA bone cement constituents.	11
TABLE 02 – Various PMMA bone cement: Ultimate compssive strength	14
TABLE 03 - Comparison: Electrochemical anodization method and rapid breakdown anodization method	35
TABLE 04 – % Cells viability based on MTT absorption results	61
TABLE 05 – PMMA composite Young's modulus	62

LIST OF FIGURES

FIGURE	<u>PAGE</u>
Figure 01 – Femur bone schematic	02
Figure 02 – Hip implant assembly	03
Figure 03 – Cemented hip implant stem	04
Figure 04 – Cementless hip implant stem of Biomet (left) and Zimmer (right)	04
Figure 05 – Schematic of cemented hip implant	05
Figure 06 – Bone cement regions indicated with red arrows	05
Figure 07 – Implant failure: improperly filled cement mantle (left) and osteolysis (ri	ght)07
Figure 08 – Normal knee anatomy	
Figure 09 – Knee implant components	08
Figure 10 – Kyphoplasty schematic_2A:insertion of device, 2B: blowing of baloon, of ballon after creating the internal cavity, 2D: filling of internal cavity b	
Figure 11 – Polymerization of PMMA	12
Figure 12 – Cell strcture schematic	18
Figure 13 - Schematic of RBA process	22
Figure 14 - Current Vs. Time behavior – RBA process of TiO ₂ nanotubes powder synthesis 0.1 M HClO ₄ electrolyte	
Figure 15 – TiO2 nanotubes in bundled form synthesized by RBA	24
Figure 16 – RBA process mechanism	31
Figure 17 – Ti foil after RBA run	
Figure 18 – Water pressure-temperature dependence of different autoclave filling fra	actions38
Figure 19 – Water dielectric constant at variation in temperature	40
Figure 20 – Schematic of exfoliation and scrolling mechanism	42
Figure 21 – FESEM images of TiO ₂ nanotubes synthesized by RBA	55

LIST OF FIGURES (continued)

<u>FIGURE</u> <u>PAGE</u>
Figure 22 – TEM images of TiO ₂ nanotubes synthesized by RBA
Figure 23 – Energy dispersion X-ray spectroscopy (EDS) spectrum of RBA TiO ₂ nanotubes56
Figure 24 – TEM images of TiO ₂ nanotubes synthesized by hydrothermal method57
Figure 25 – XRD pattern of as-synthesized and calcined (400°C for 5 hours) hydrothermal TiO ₂ nanotubes
Figure 26 – Energy dispersion X-ray spectroscopy (EDS) spectrum of hydrothermal TiO ₂ Nanotubes
Figure 27 – FESEM image of Ag-HA nanobelts
Figure 28 – MTT assay absorbance results
Figure 29 – Stress Vs. Strain curve: comparison between Pure PMMA, PMMA with 2.5wt% TiO ₂ nanotubes as filler and PMMA with 2.5 wt% Ag-HA nanobelts as filler62
Figure 30 – Ultimate compressive strength (MPa)63
Figure 31 – Disc diffusion inhibition zone method (a) TiO ₂ nanotubes powder pallet and (b) Ag-HA nanobelts powder pallet

SUMMARY

Bone cements are being used over decades for various arthroplasty surgeries. Polymethylmethacrylate (PMMA) is commonly used bone cement known for its better mechanical strength in comparison with state of the art other bone cements calcium sulfate (Cas) and calcium phosphate (CaP). To achieve higher mechanical strength in comparison with cortical bone, efforts have been taken for past two decades with the addition of various filler materials. Still existing PMMA bone cements have limitations over its sufficient mechanical strength and lacking bioactivity. This research work suggests potential filler materials which can enhance mechanical strength and simultaneously can provide bioactivity to promote cells growth. Titanium dioxide nanotubes (TiO₂) synthesized by hydrothermal method have advantages over individuality and higher surface area as compared with other filler materials. On the other hand, silver doped hydroxyapatite (Ag-HA) nanobelts have their unique advantages being able kill bacteria and promoting cells growth simultaneously which ultimately a crucial aspect for osteointegration after placing an implant. Also flexibility of these nanobelts is an advantage for enhancing mechanical strength of PMMA bone cement. This study displays comparative study of PMMA bone cement with the incorporation of TiO₂ nanotubes and Ag-HA nanobelts as fillers. To investigate the effect on mechanical strength, compression test is performed as per ISO5833 standard. To evaluate the cytotoxicity and bioactivity, (3-(4,5-dimethylthiazol-2-yl)-2,5diphenyl tetrazolium bromide) MTT cells viability assay is performed. Additionally, anti-bacterial test is carried out to evaluate the effect of respective filler materials at specific weight percent. Finally, the significance of current research work has been explained along with the scope for further developments.

1. INTRODUCTION

1.1 Bone cements:

Most of the clinically approved state of the art bone cements are based on polymethylmethacrylate (PMMA). CMW1, Surgical Simplex, Palacos® are the examples of commercial commonly used PMMA based bone cements (1). Bone cements based on calcium sulfate (CaS) and calcium phosphate (CaP) are also being studied as potential substitutes for PMMA based bone cements, but still there are certain concerns about their biomechanical properties. The main drawback of CaS bone cement is its rapid degradation rate which cannot support augmented bone sections for long and that with CaP bone cement is its slow degradation rate which interrupts bone regeneration process (2). Efforts have also been taken on glassionomeric cements considering their advantage of the absence of polymerization process heat dissipation, but they lack in sufficient mechanical strength (3).

Various reasons for bone surgeries are osteoarthritis (breakdown of cartilage joint, that is the lack of cushioning at the end of the long bone), rheumatoid arthritis (inflammation of joints causing immobility), avascular necrosis (death of bone tissues due to insufficient blood supply) and osteoporosis (brittleness of bone tissues due to lack of vitamin D or calcium) (4). Arthroplasty is the surgical procedure to replace or reorient the existing joints in the human body with the artificial implants (5). Various arthroplasty surgeries are associated with hip joint, knee joint, rarely with shoulder joint, thumb joint and for spinal cord vertebroplasty and kyphoplasty.

The following section includes the significance of bone cement in the total hip arthroplasty surgeries.

1.2 Total hip arthroplasty (THA):

According to American Joint Replacement Registry (AJRR) 2017 report, in 2016 there were total 277200 hip arthroplasty surgeries of all kinds in the United States out of which 23839 were revision surgeries (6). This also implies that the revision hip surgeries had imposed the burden of around 8.6%. Also study shows that the total hip arthroplasty surgeries are more dominant in women with respect to men population. Considering this trend, total hip arthroplasty surgeries will continue to rise exponentially and is expected to hit the number of 4 million by 2030 (7). The hospital cost of hip replacement surgery varies between \$22500 - \$126000 (8).

1.2.1 Femur bone in human body:

Hip arthroplasty surgery is related to the femur bone and its joints near pelvis in human body. Femur bone is called as thigh bone which is the longest and heaviest bone in human body.

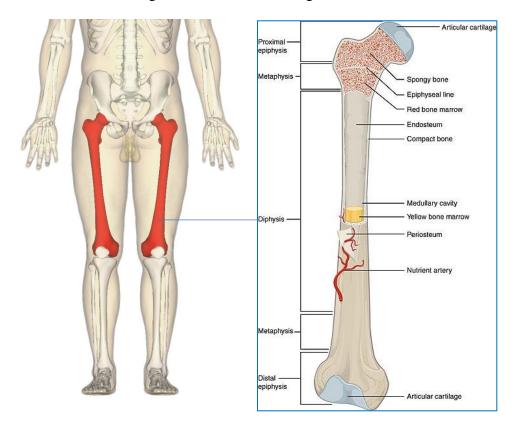
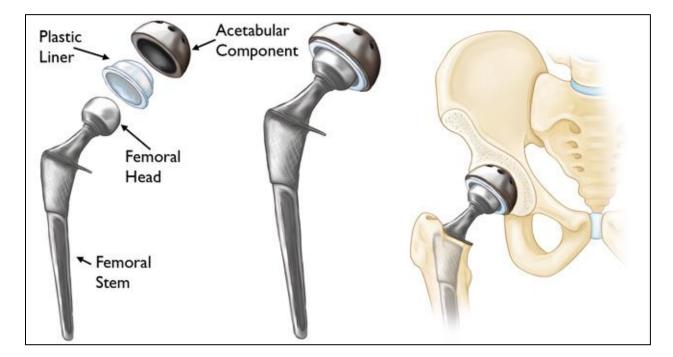


Figure 01 - Femur bone schematic (9,10)

The head of the femur bone is smooth and spherical which forms ball and socket hip joint with the cup shaped acetabulum of the hip bone near pelvis (11). Rounded shape of the head allows rotational motion in any direction. At distal end which is wide is connected to the knee portion of a body. The surfaces at both the ends of the femur bone are known as articulate cartilage which are very smooth and flexible as they form joint links. The end portions of a long bone are known as the cancellous bone or spongy bone and these bone tissues are responsible for producing blood cells (12). The middle long and hard portion of the bone is known as cortical bone or compact bone. The cortical bone portion is very strong and hence it is hard to get fractured as compared with cancellous bone. The central part of cortical bone consists of central canal contained with blood vessels, nerves and bone marrow.



1.2.2 Hip implant assembly and locations of bone cement applications:

The hip prosthesis consists of a femoral stem, a femoral head attaching the stem and acetabular cup with the liner which gets fixed in the acetabulum in the pelvis (14).

Figure 02 – Hip implant assembly (13)

There are mainly two categories of hip implants depending upon hip arthroplasty with bone cement and without bone cement.

1. Cemented hip implant stem:



Figure 03 – Cemented hip implant stem (15)

2. Cementless hip implant stem:



Figure 04 – Cementless hip implant stem of Biomet (left) and Zimmer (right) (16)

In cemented hip implant arthroplasties, bone cement is applied at following two locations:

- 1. Fixation of stem with femur bone
- 2. Fixation of acetabular cup with acetabulum

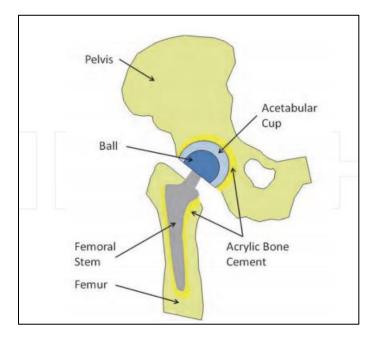


Figure 05 – Schematic of cemented hip implant (17)



Figure 06 – Bone cement regions indicated with red arrows (3)

1.2.3 <u>Reasons for revision hip surgeries – hip implants failure:</u>

The reasons for revision hip implant surgery are improper hip prosthesis design, improper fixation of implant with bone cement, materials handling and additionally patient's age and activities (14). Revision surgeries are very complex and time consuming considering difficulty in removing earlier fixed implant and longer anasthesia period. The main reason for implant failure is aseptic loosening of implant (14). One of the cause of loosening of implant is microparticles formed as a result of the continuous frictional motion between articulate cartilage and acetabular cup (18). These particles promote osteolysis. "Osteolysis is defined as the process of progressive destruction of periprosthetic bony tissues". Also, micromotion between implant and bone can ultimately lead towards implant failure. In the case of uncemented hip implants, elastic properties differs widely between bioflexible cortical bone and rigid metal implant which leads to the thigh pain for the patients (19).

The reasons for failure of cemented hip implant can be summarized in relation with applied bone cements. Successful application of bone cement is highly dependent on surgeon's skills. Proper mixing before fixing cement is very crucial in order to carry out uniform polymerization process. The failure may occur between cement-stem and cement-bone interfaces as a result of interfacial stresses and micromotion (20). Also, state of the art bone cements have comparative compressive strength, but their tensile strength and shear strength are still low. Also, cracks formed after complete polymerization cause the failure of implant by reducing its fatigue life (21). Additoinally, cement layer thickness and uniform filling affect the success rate of hip arthroplasty surgery (3).

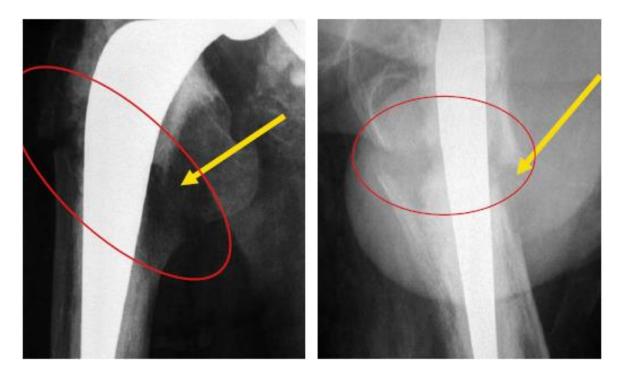


Figure 07 – Implant failure: improperly filled cement mantle (left) and osteolysis (right) (3)

1.3 Total knee arthroplasty:

By referring to American Joint Replacement Registry (AJRR) 2017 report, in 2016 there were total 480581 knee arthroplasty surgeries in the United States (6). Among these 24509 were revision surgeries which signifies the burden of 5.1%. The main causes of total knee arthroplasty (TKA) surgeries are osteoarthritis (wear and tear cartilage portion of bone), rheumatoid arthritis (related to inflammation of joints) and post-traumatic arthritis (tearing of knee ligaments causing malfunctioning of knee (108).

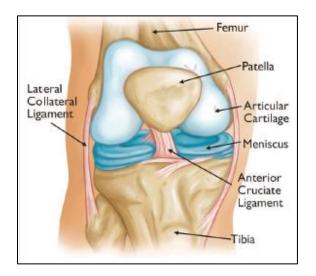


Figure 08 – Normal knee anatomy (107)

Knee implant has three main components: femoral metal component at the end of femoral bone cartilage, tibial metal component inserted in the tibial cartilage side and a medical grade plastic spacer which works as cushioning between two metal components. Bone cements are applied between implant metal components and bone interfaces.

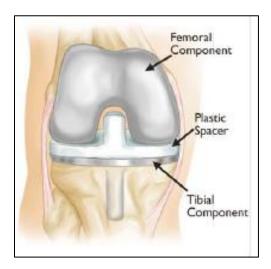


Figure 09 – Knee implant components (107)

The reasons for the failure of total knee surgeries are related to the aseptic loosening of implants due to repetitive heavy activities which are more associated with the insufficient

mechanical strength and cells proliferation rate provided by bone cements, improper implant fixation and prosthetic joints infections.

1.4 <u>Need for improvisation of the state of the art bone cements:</u>

The statistical data of aforementioned total hip arthroplasty (THA) and total knee arthroplasty (TKA) comprehensive studies clearly indicate the need to improve biomechanical properties of state of the art bone cements. Also, as per American Joint Replacement Registry (AJRR) report, the annual number of total knee arthroplasty surgeries is higher than total hip arthroplasty surgeries (6). If we consider the statistical annual number of arthroplasty surgeries for hip, knee and thumb and that for kyphoplasty and vertebroplasty, the importance of bone cements will be merely significant. In order to minimize complex revision arthroplasty surgeries which are extremely costly, time consuming and painful for the patients, there is extreme need to improvise state of the art bone cements with respect to their bioactivity and mechanical properties.

2. POLYMETHYLMETHACRYLATE (PMMA) BONE CEMENT COMPOSITES 2.1 <u>Overview:</u>

The primary role of polymethylmethacrylate (PMMA) bone cement is to transfer body weight during static or dynamic activities from implant to bone without any disruption at implant-bone cement-bone interfaces (22). Stresses generated are distributed through implant-bone cement-bone connections. As mentioned earlier, PMMA bone cements have wide variety of applications in different hip, knee, thumb and vertebra arthroplasty surgeries. In vertebra arthroplasty surgeries, vertebroplasty and kyphoplasty are considered as modern arthroplasty techniques (23).

Kyphoplasty and vertebroplasty are mainly caused as a result of osteoporosis. Vertebroplasty is nothing but the application of low-viscosity injection of PMMA to stabilize the spine which can stop the pain but cannot recover the deformation of the spine (24). While kyphoplasty is the minimum invasive technique which can fix painful vertebra compression fractures internally and can regain original shape of vertebra (24). In both the cases viscosity of PMMA is very crucial. The viscosity of PMMA is usually altered by changing the molecular weight and by changing the ratio of constituents (25). The cement should be a liquid during its working polymerization phase in order to flow through delivery device to penetrate through cancellous bone by achieving proper interlock with vertebra (23).

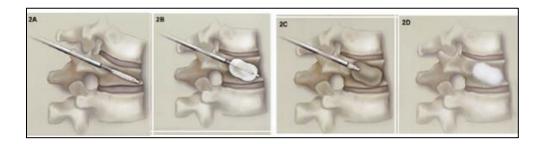


Figure 10 – Kyphoplasty schematic_2A:insertion of device, 2B: blowing of baloon, 2C: removal of ballon after creating the internal cavity, 2D: filling of internal cavity by PMMA (24)

This section includes PMMA bone cement compositional details along with its polymerization process, mechanical properties as a result of various filler materials and its critical limitations. Additionally, cytotoxicity and anti-bacterial studies of PMMA bone cement are described in comprehensive way.

2.2 PMMA bone cement composition and polymerization process:

The contents of PMMA bone cement consists of two main phases as powder and liquid. In addition to PMMA powder, it contains initiator as benzoyl peroxide for radical polymerization. Radiopacifier and antibiotic are also included in the powder form. Methyl methacrylate is the main liquid monomer. Additionally, as an activator N,N -dimethyl p-toluidine and to prevent premature polymerization during storage as inhibitor hydroquinone are used (3).

Sr. No.	Phase	Contents	Purpose
01		Polymethylmethacrylate (PMMA)	Main polymer
02	Powder	Benzoyl peroxide (BPO)	Initiator – radical polymerization
03		Zirconium dioxide (ZrO ₂)	Radiopacifier – X-ray monitoring
04		Gentamicin	Antibiotic – to inhibit bacterial growth
05		Methy methacrylate (MMA)	Main liquid monomer
06	Liquid	N,N -dimethyl p-toluidine (dMpT)	Activator – for forming radicals
07		Hydroquinone	Inhibitor – to prevent premature polymerization during storage

Primarily, radical polymerization of BPO intiator and dMpT activator occurs at room temperature. The decomposition of BPO takes place due reduction/oxidation reaction by electron transfer resulting in benzoyl radicals (3). These free radicals react with C=C of MMA which causes to form long radical chains. Recombination of these radical chains ends the polymerization and increases the viscosity of the bone cement.

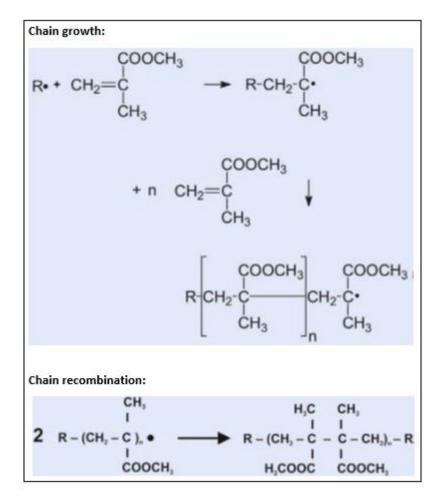


Figure 11 – Polymerization of PMMA (3)

The powder to liquid ratio plays an important role in polymerization process. With lower powder to liquid ratios the proxide/amine ratio will also get reduced causing more rate of decomposition of peroxide by forming more number of peroxide radicals and hence terminating the polymerization process quickly which ultimately increase the residual monomer (26). If this ratio is too low or too high, it will make cement either too stiff or too diluted liquid, which is not suitable for clinical applications.

2.3 Mechanical properties of PMMA bone cements:

The standard which is used currently to control and maintain the minimum requirements of PMMA bone cement is ISO5833 (3). According to the ISO standard the mechanical properties of cured bone cement should be: compressive strength minimum as 70 MPa, bending modulus minimum as 1800 MPa and bending strength minimum as 50 MPa. Compressive strength of PMMA bone cement is usually around 70% of cortical bone. Compression strength of non-osteoporatic cortical bone is 131 MPa and that of cancellous trabacular bone is 4-12 MPa (27).

- Properties of PMMA bone cement at laboratory testing (3,23):
 - 1. Ultimate tensile strength: 36 to 47 MPa
 - 2. Ultimate shear strength: 50 to 69 MPa
 - 3. Ultimate compressive strength: 70 to 94 MPa
 - 4. Bending strength: 67 to 72MPa
 - 5. Bending modulus: 2552 MPa

Sr. No.	Filler material	Composition wt%	Ultimate compressive strength
01	HA powder and	PMMA (50%) + HA	Control PMMA: 94 MPa
	Chitosan powder (28)	(40%) + Chitosan (10%)	PMMA+HA+Chitosan: 82 MPa
02	200 nm particles-	$PMMA(50\%) + TiO_2$	Control PMMA: 84 MPa
	TiO ₂ powder (29)	particles (50%)	PMMA+TiO ₂ : 70 MPa
03	Mesoporous silica	PMMA (95%) +	Control PMMA: 85.9 MPa
	particles (30)	mesoporous silica (5%)	PMMA+Silica: 89.5 MPa
04	Multi-walled carbon	PMMA (99%) +	Control PMMA: 59.8 MPa
	nanotubes (31)	MWCNT (1%)	PMMA+MWCNT: 66.8 MPa
05	Collagen ~200 µm	PMMA (95%) +	Control PMMA: 90 MPa
	(32)	collagen (5%)	PMMA+Collagen: 88 MPa

TABLE 02 – Various PMMA bone cement: Ultimate compssive strength

As long as filler material reinforced PMMA bone cement is achieving compressive strength of 70 MPa, it can be considered as for clinical applications (32).

2.4 Limitations of PMMA bone cement composites:

Ideal bone cement should possess charactristics like ease of handling, high radiopacity, required optimum viscosity, low curing tempearture, uniform optimum mechanical properties, biocompatibility, bioactivity, low price and slow bio-degradation (33). Even though PMMA is widely used bone cement composite, there are certain disadvantages of PMMA for which studies are being carried out in order to overcome these limitations with the help of various filler materials. Critical disadvantages of PMMA bone cements are listed below:

2.4.1 <u>High curing temperature:</u>

The radiacal polymerization of PMMA and MMA is a exothermic chemical reaction (3). With time, as polymerization proceeds, dough viscosity also increases releasing heat of polymerization

quantified as 57 kJ per mole MMA (3). This polymerization heat causes necrosis of implant connecting tissue which leads towards aseptic loosening of implant. This temperature peak with in-vivo study has shown value as 40°C-46°C at bone cement interface (3). This temparture peak can be reduced slightly either by changing powder to liquid ratio or with higher radiopacifier content.

2.4.2 Factors affecting mechanical strength of PMMA:

Implant-cement and cement-bone interfaces are considered to be the 'weak link zones', as the significant variation in stiffnesses in implant, bone cement and bone occurs (22). If the bonding between these interfaces is not properly achieved as a result of may be non-uniform or low cement thickness, this can lead towards aseptic implant failure due to loosening. Also, shear strength of PMMA bone cements is not at its desired extent, which also can form cement debris causing detachment of bone-implant interface connecting tissues. Inadequate polymerization due to improper mixing of PMMA bone cement constituents can cause cracks which ultimately is the responsible factor for reduced mechanical strength of bone cement.

2.4.3 Chemical necrosis:

Release of liquid monomer MMA as a result of incomplete polymerization or excess untreated monomer can cause cells death at bone-implant interface which is known to be a probable cause for chemical necrosis (22).

2.4.4 Lacking bioactivity:

PMMA cement lacks bioactivity inherently which causes lack of integration of bone tissues with surgical implants (34). Hence, filler materials like hydroxyapatite plays cruicial role in promoting superior osteoconductive and osteoinductive properties.

2.4.5 Insufficient radiopacity:

Pure PMMA lacks sufficient radiopacity which causes difficulties to surgeons during X-ray scanning to locate exact implant and cortical bone areas (35). Therefore, radiopacifiers like barium sulfate and zirconium dioxide are added to PMMA bone cements.

2.5 <u>PMMA bone cement – bone cells interaction:</u>

Before understanding intercation between PMMA bone cement and bone cells, it is important to have brief overview of bone cells and their proliferation mechanism.

2.5.1 Bone extracellular matxix:

Bone matrix consists of inorganic salts and organic matrix (36). Organic matrix consists of collagenous protein and non-collagenous proteins like fibronectin and osteonectin. Inorganic material of bone matrix is enriched with calcium and phosphate ions along with bicarbonates, magnesium, sodium, potassium, citrate, fluorite, zinc, barium, strontium. Hydroxyapatite crystals are nucleated from calcium and phosphate ions which are deposited on scaffold synthesized by collagen and non-collagenous matrix (37). This interaction defines stiffness and resistance of bone tissues. Bone cells and bone matrix interaction occurs via molecules, mainly because of integrins (36).

2.5.2 Bone cells:

Bone is mineralized connective tissue mainly possess four types of cells: osteoblasts, bone lining cells, osteocytes and osteoclasts (36). The role of each of this cells line is described briefly as follows:

1. Osteoblasts:

These are bone forming cells and they synthesize proteins mainly collagens. Their population is about 4-6% on bone matrix.

2. Bone lining cells:

Bone lining cells are flat cells which cover bone surface. They don't contribute in bone resrption or formation. The main function of these cells is to prevent unnecessary interaction between osteoclasts and bone matrix.

3. Osteocytes:

The population of osteocytes is 90-95% and these are long-lived cells. Osteoblasts are converted to osteocytes at the end of bone formation cycle. Main fuction of these cells is to regualte the activities of osteoblasts and osteoclasts in order to maintain proper functionality of bone and other organs (38).

4. Osteoclasts:

These are multinucleated cells which are responsible for bone resorption. They compete with bone forming osteoblasts cells. They release enzymes which breakdown the bone. They process this bone debri and further break it down to proteins and calcium and phosphate ions which are utilized by other parts of the body.

2.5.3 PMMA- MTT cells viability assay:

PMMA in its intial period induces certain cytotoxicity till it gets stabilized. The reasons associated with this are powder to liquid ratio and polymerization process (39). Hence, it is important to study cytotoxicity of PMMA bone cements. (3-(4,5-dimethylthiazol-2-yl)-2,5diphenyl tetrazolium bromide) MTT assay is the easiest and approximate in-vitro way of masuring viable cells. The working principle of MTT is briefly described as follow:

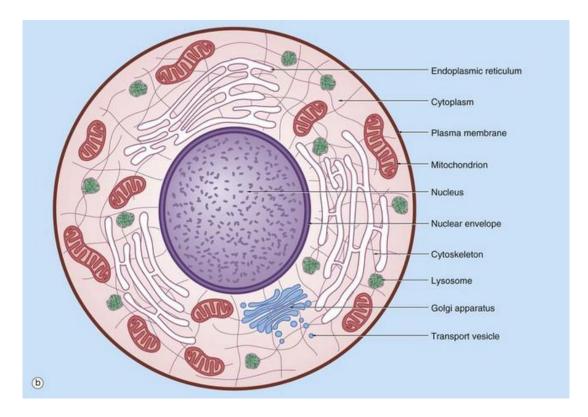


Figure 12 – Cell strcture schematic (40)

Mitochondria in viable cells is responsible for metabolism which converts this MTT into purple colored insolublized formazan salts. Only viable cells can form this product, once cells die they loose their ability to form these formazan salts. Hence, more number of viable cells will produce more quantity of these salts which can be considered as comparative measure. Then dimethoxy sulfoxide (DMSO) is added to solublize these formazan crystals in absence of light. Subsequently, this cells media with DMSO is checked under UV spectrometer at 570 nm wavelength to evaluate absorbance (41).

2.6 PMMA – antibacterial studies

Bacterial infection is the critical issue associated with implant surgeries. Main reason is the adhesion of bacteria at implant-bone cement-bone interfaces. Main factors influencing bacterial

infection are environmental factors, bacterial properties, material surface properties, presence of proteins at interfaces, chemical composition of material, surface roughness and surface charge (42). Staphylococcus bactaerial species is highly occupy pathogenic population which is the main cause for septic arthritis. In addition to Staphylococcus aureus, Escherichia Coli and Streptococcus sanguinis bacterial species are considered for in-vitro studies.

As PMMA bone cement doesn't possess any antibacterial properties, hence gentamicin sulfate is added to it as an antibiotic. It can inhibit the growth of gram-negative and gram-positive bacteria. Gentamicin damages bacteria cell membrane which apparently kills bacteria as a result of malfunction of cell membrane (43). Silver ions can inhibit the growth of gram-negative and gram-positive bacteria by causing structure changes to cell membrane and by damaging it (44). Hence, silver doped filler materials are being incorporated in PMMA bone cements to provide antibacterial characteristics.

2.7 Importance of TiO2 in biomedical field:

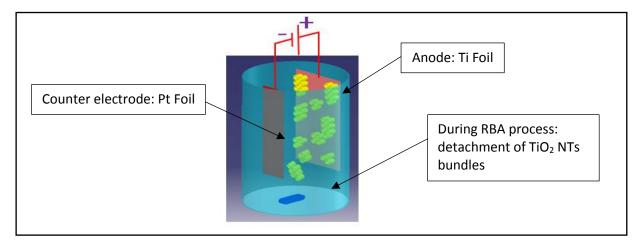
Over last two decades, a lot of research has been performed on TiO_2 in order to explore its properties and applications in biomedical field. TiO_2 has excellent advantages associated with photocatalytic activity in presence of UV light which makes it suitable for clinical antibacterial applications. Additionally, TiO_2 excellent biocompatibility, corrosion resistance and good mechanical properties (45). Besides synthesis of high aspect ratio TiO_2 nanomaterials can be achieved with comparatively less complicated and economical synthesizing methods. TiO_2 nanotubes grown on the implant surfaces have advantages like improved cells adhesion (46). Also, TiO_2 nanofibers can provide higher radiopacity which is important for bone cement applications (47). Hydrothermal TiO2 nanotubes are explored for drug delivery applications due to their high surface area, individuality and high surface energy (48).

3. TiO₂ NANOTUBES SYNTHESIS BY RAPID BREAKDOWN ANODIZATION (RBA) METHOD

3.1 Overview:

Rapid breakdown anodization (RBA) is the fastest and the cost-effective method for the synthesis of high aspect ratio TiO_2 nanotube bundles in the powder form. The reaction kinetics of RBA are ultrafast and as-synthesized nanotubes lacks in the self-organization and uniformity due to the use of non-fluoride electrolyte species like chloride (Cl⁻) and perchlorate (ClO₄⁻) (49). In general, the setup looks like the electrochemical anodization, but the stepping potential is applied across the electrodes instead of sweeping potential and the passivity breakdown conditions are achieved within one minute and hence nanotubes bundles are released from the titanium foil periodically. Applied potential and the electrolyte species are the most critical factors to achieve these localized passivity breakdown conditions (49,50).

This section includes the detailed understanding of RBA process with respect to its reaction mechanism, critical process parameters and reasons for releasing of TiO₂ nanotubes bundles in the electrolyte. Additionally, corrosion aspects of RBA process are explained in detail. Also, brief comparison between electrochemical anodization process and RBA process has been included at the end of the section.



3.2 Rapid breakdown anodization – reaction mechanism understanding:

Figure 13 - Schematic of RBA process

The RBA process mechanism can be explained comprehensively with the help of its current

Vs. time transient behavior.

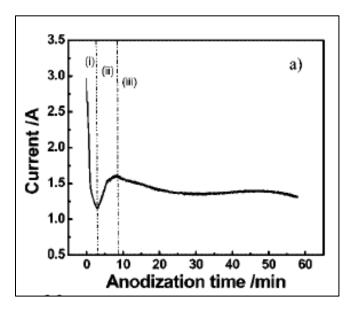


Figure 14 - Current Vs. Time behavior – RBA process of TiO_2 nanotubes powder synthesis at 20 V in 0.1 M HClO₄ electrolyte (49)

The current Vs. time transient plot displays three main regions (49) (50):

Region (i) – initial exponential decay: This initial decay causes due to the initial oxidization of Ti foil and hence formation of compact layer of TiO_2 which apparently obstructs the rate of the transfer of ions in the electrolyte.

At anode, oxidation of metal:

$$Ti \longrightarrow Ti^{4+} + 4e^{-}$$
(01)

With electric field, water breaks down:

$$H_2O \longrightarrow H^+ + OH^-$$
(02)

 $OH^{-} \& O^{2-}$ combines with Ti^{4+} ions:

$$Ti^{4+} + 2O^{2-} \longrightarrow TiO_2$$
(03)

Overall anodic reaction:

$$Ti + 2H_2O \longrightarrow TiO_2 + 4H^+ + 4e^-$$
 (at anode) (04)

Region (ii) – gradual increase in the current: This region indicates gradual dissolution of titanium dioxide layer by chloride ions. This is achieved at sufficiently high voltage causing strong electric field breakdown conditions limiting the growth of TiO_2 and inward migration of oxide layers occur causing oxidation of Ti foil as well as dissolution of TiO_2 at electrolyte/oxide interface.

Pit formation reaction:

$$TiO_2 + 6Cl^- \longrightarrow (TiCl_6)^{2-} + 2H_2O$$
(05)

Region (iii) – steady region: This region denotes steady simultaneous reaction of oxidation and dissolution. This region keeps following the cycle of passivation and pits formation with the release of length of grown TiO_2 nanotubes.

At cathode: (intense evolution of hydrogen)

 $4H^+ + 4e^- \longrightarrow 2H_2^{\uparrow}$

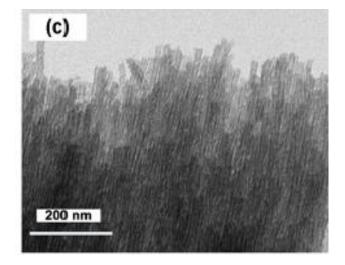


Figure 15 – TiO2 nanotubes in bundled form synthesized by RBA (51)

3.3 Rapid breakdown anodization process parameters:

This section mainly focuses on the understanding of RBA process from electrochemistry perspective.

3.3.1 Effect of the applied potential:

Commonly used applied potentials are sweeping (electrochemical anodization) and stepping (rapid breakdown anodization). In electrochemical anodization process, applied potential is very important parameter, as it controls the ion migration within metal/metal oxide interface (50). There is a linear relationship between applied voltage and nanotubes diameter till 60 V (50,52). In the case of rapid breakdown anodization, stepping voltage is applied instead of sweeping. When stepping voltage is applied, electric field strength is higher and as a result breakdown events occur (53). Stepping voltage is the main cause for the localized dissolution of

(06)

current resulting in the pitting corrosion (54). Specific areas of foil surface are activated and high current density can be established. In RBA, applied potential doesn't control the diameter of the nanotubes, but it affects the number of nucleation sites on the foil (50).

3.3.2 Effect of the electrolyte species:

Electrolyte species define the morphology of the nanotubes. Fluoride ions containing electrolytes possess high density of nucleation sites and pore initiation is achieved by field assisted dissolution (50). As a result, uniform nanotubular arrays can be obtained in the organic electrolytes. While in fluoride ions containing aqueous electrolytes, dissolution rate is hard to control, but high density of nucleation cites is equally present on the titanium substrate (50).

RBA occurs in the presence of chloride, bromide and perchlorate ions. The process is initialized due to localized breakdown of anodic films (50). Self-organization of TiO₂ nanotubes cannot be achieved in the electrolytes containing Cl⁻, Br⁻ and ClO₄⁻ ions (55). Chloride ions are quite aggressive and the main cause of pitting corrosion i.e. passivity breakdown conditions are achieved (53,56). The ionic radii of halide ions are also a critical factor which varies like $\Gamma > Br^-$ > Cl⁻. Smaller the ion more aggressive it will be for passivity breakdown (57). Ionic radius of fluoride ions is smaller than that of chloride ions, but fluoride ions can form strong metal-fluoride bonds and as a result heavy localized dissolution occurs than localized pitting corrosion (58). The shape, size and the depth of pits formation depend upon the concentration of chloride ions (59).

3.3.3 Effect of the electrolyte pH:

The electrolyte pH is the crucial parameter in the rapid breakdown anodization method, as it affects chemical dissolution rate of titanium dioxide layer. At low pH, titanium oxide dissolution rate is higher than that at neutral electrolyte pH (60). The acidity of the electrolyte influences dynamic equilibrium process of field assisted chemical dissolution and oxidation of titanium (61). When a surface with oxide layer is immersed in the aqueous solution, the surface charge is developed mainly because of electronegativity of cations in the material and the pH of the solution (62). The nanotubes length decreases at lower pH values. For electrolyte pH < 4, microscopic pits can be eliminated (63). By reducing the pH, the viscosity of the electrolyte decreases. As a result, nanotubes can be grown at faster rate. With increase in pH, the hydrolysis products increase and hence the rate of chemical dissolution slows down, apparently the time required to reach equilibrium of nanotubes formation and dissolution rate increases (64). Hence, for the synthesis of TiO₂ nanotubes by RBA method, electrolyte pH remains within the acidic range, at 4.4 when using chloride ions or at 1.81 while using perchlorate ions.

3.3.4 <u>Effect of the electrolyte temperature:</u>

The applied potential can alter the process kinetics during the rapid breakdown anodization, as during the anodization process, it is the responsible factor for the change in the electrolyte temperature. When compared at the room temperature, for 20 V, the electrolyte temperature increases by 15°C to 18°C, whereas the same for 10 V applied voltage, temperature increases by only 3°C (65). The relative large rise in the electrolyte temperature at 20 V applied is attributed to the significantly increased current. When anodization is carried out at low temperature, the drastic change in the reaction kinetics is observed as oxidation and breakdown process gets a lot slower (50) (66). The variations in the electrolyte temperature and the applied potential do not affect the morphology of the nanotubes, but they affect the growth rate (49). For decreased electrolyte temperature and decreased applied potential, the growth rate decreases.

According to the Stokes-Einstein relation (66):

$$D = \frac{kB \times T}{C \times \pi \times \eta \times \sigma} \tag{07}$$

kB - Boltzmann Constant

- T electrolyte temperature
- C numerical constant determined by the hydrodynamic boundary condition
- σ diameter of the hard sphere particle
- D diffusion coefficient

η – the solution viscosity

The Stokes-Einstein equation shows that the diffusion coefficient is directly proportional to the electrolyte temperature and inversely proportional to the viscosity of the electrolyte (66). With increase in temperature, the viscosity of the electrolyte decreases and a result process kinetics changes by faster drift velocity of ions. This also increases dissolution rate of the oxide film. The current density increases with the increase in the electrolyte temperature which also proves increase in the diffusion coefficient (66) (67).

3.3.5 Effect of the counter electrode material:

The counter electrode material plays significant role in controlling the electrolyte activity during anodization process. Allams et. al. stated that the overpotential of the cathode material is an important factor that affects the dissolution kinetics of the Ti anode (68). Higher the number of dissolved Ti^{4+} ions in the electrolyte, higher will be the conductivity of the electrolyte and hence higher ion transport rate (67) (68). This affects the overall reaction rate and hence the morphology of the nanotubes. The stability of the cathode is defined in terms of the cathode mass loss rate (mg/cm²/h) (68).

$$R = \frac{(W1 - W2)}{(A * t)} \tag{08}$$

W1-weight of the cathode material before anodization

W2 – weight of the cathode material after anodization

A – the surface area of the cathode material

t – anodization time

The stability of the different cathodic materials in aqueous electrolytes:

 $Pt \sim Pd > C > Ta > Al > Sn > Cu > Co > Fe > Ni > W$

Platinum and Palladium materials possesses highest stability considering zero mass loss during the anodization process in aqueous electrolytes (67) (68). Platinum nanoparticles have substantial properties like high surface area, high transmittance, low charge transfer resistance and high electrical conductivity. The high surface area promotes higher number of nucleation sites available for the redox reaction which results in the increased current density (69). Carbon cathode materials are cheaper alternative replacement for platinum electrodes considering their good chemical stability, electrical conductivity and catalytic activity (67) (69).

3.3.6 Effect of the electrodes surface area:

The counter electrode surface area is a critical factor, as it controls the reaction rate during rapid breakdown anodization process. As discussed earlier, hydrogen evolution reaction occurring at cathode is an important part of RBA mechanism. To maintain the proton reduction rate, it is essential to have counter electrode that can provide numerous nucleation sites. Enhanced hydrogen evolution at cathode ensures high reaction rate promoting enhanced pits formation at anode (50,67). The electrodes surface area is one of the key aspects for increasing the current intensity which is highly vital during rapid breakdown anodization process.

The effect and importance of large cathodic surface area can be understood with the help of the mass transport phenomenon during anodization process. Diffusional transport takes place at the vicinity of the electrode surface. The flux of electroactive species to electrode is completely due to diffusion phenomenon. Migration transport mainly plays role in the bulk electrolyte (70). Hence, Ti positively charged electrode surface area as well as surface characteristics (mainly surface roughness) are responsible for the distributive nucleation sites on the Ti substrate during applied stepping voltage. Also, this is the probable reason for the closer and irregular nucleation sites which are responsible for non-uniform nanotubes bundles formation at anode.

3.3.7 Effect of the magnetic stirring:

The magnetic stirring is the forced convection mode of mass transport and can transport solutes towards the electrode (71). Stirring during RBA process, increases the reaction rate. It can reduce the overall process time by 50% (49). Also, stirring of the electrolyte keeps the bath temperature of the electrolyte uniform during the process (72). Magnetic stirring is crucial for increasing the flow of ions in the electrolyte which supports the rapid reaction kinetics of the process.

3.4 Understanding of rapid breakdown anodization process with corrosion aspects:

In RBA process, stepping voltage is the driving parameter that makes certain areas of Ti foil highly charged. These areas act as nucleation sites for the localized pits formation. Pitting corrosion is the main aspect of RBA process. In this section, film breakdown mechanism of pits formation is briefly explained. Additionally, the reasons for releasing of nanotubes bundles from the Ti substrate are mentioned in the concise manner.

Film breakdown mechanism of pits formation:

Pits are generally formed by the rupture of passive film by giving direct access to aggressive anions towards the unprotected metal surface (59). These cracks or openings can be caused within the oxide film by electrostriction stress, surface tension, plastic deformation of oxide film by oxygen bubbles evolution at anode and blistering of metal surface (50) (73).

Oxygen bubble gets trapped within the metal oxide surface generates plastic deformation of oxide film and as a result non-uniform oxide layer is formed. Additionally, surface microscale roughness also contributes to the non-uniform oxide layer. There are some studies which mention Cl⁻ ions penetrate easily through concave section of surface roughness where electric field strength is comparatively high (59). Compressive strength of the oxide film gets reduced with the penetration of Cl⁻ ions.

The pressure varies across the thickness of the oxide film. Two main reasons for the variation of pressure are electrostriction force and surface tension (74).

$$P - P_0 = \frac{\varepsilon (\varepsilon - 1) E^2}{8 \pi} - \frac{\gamma}{d_{crit}}$$
(09)

P – Pressure across the oxide film thickness

P₀ – Atmospheric pressure

 ϵ – dielectric constant of the film

 γ – surface tension

d_{crit} – critical thickness of the oxide film

Adsorption of aggressive anions like Cl⁻ reduces the surface tension of oxide film suddenly which will promote the mechanical breakdown at lower applied potentials when film thickness is

minimum (49) (50) (59). Rapid process kinetics also contributes to the detachment of nanotubes from the substrate.

Rapid breakdown anodization process – proposed reaction mechanism:

Above sections help us to understand rapid breakdown anodization process in general, various factors governing the process and the role of pitting corrosion in the process. This section provides in-depth proposed insights over the reactions occurring near electrodes surfaces, the reasons behind random pitting corrosion sites on Ti foil and the role of stepping voltage in the RBA process. The reaction mechanism of rapid breakdown anodization process can be defined by considering electrochemistry and corrosion aspects. (Please refer representative schematic)

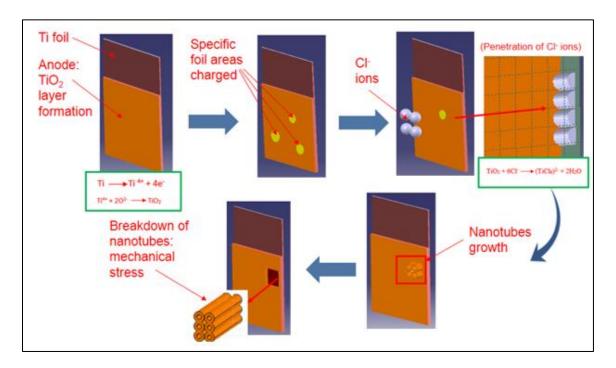


Figure 16 – RBA process mechanism

This representative schematic shows main stages of the RBA reaction. Briefly as soon as stepping voltage is applied, titanium dioxide layer is formed on the Ti foil. Specific areas of the foil are highly charged which are more prone to the pitting corrosion sites. Following to it, chloride ions from the electrolyte react aggressively to penetrate the oxide layer and result in the formation of pits. At the same time along with the dissolution of oxide layer, oxide layer continues to grow which ultimately defines the lengths of the nanotubes. In the highly acidic aqueous solution, the dissolution rate is more dominant than oxidation rate, as a result of which synthesized nanotubes average length stays restricted till 5-7 μ m. At the end, due to the volumetric expansion of oxide layer and non-uniform oxide layer formation in addition to highly dynamic reaction kinetic generate the mechanical stress which causes the release of TiO₂ nanotubes bundles during RBA process.



Figure 17 – Ti foil after RBA run

The proposed reaction mechanism at electrode/electrolyte interface can be explained as follows: Stepping voltage promotes the double layer formation at electrode/electrolyte interface. As a result of which Cl⁻ ions are readily present at anode as soon as stepping voltage is applied. With applied voltage passive oxide layer is formed on the Ti foil instantaneously. But, at the same time, chloride ions also have high reactivity due to smaller ionic radius and aqueous electrolyte with very less viscosity. Electrode surface contains microscale surface roughness which is the main reason for irregular oxide layer across the electrode/electrolyte interface. Also, electrolyte species get trapped in the oxide layer and metal impurities can form oxide layer interruptions which results in the non-uniform oxide layer. Studies also suggests that the concave portion of the oxide surface roughness with thinner thickness is more prone to pitting corrosion site. During passivation stage volumetric expansion stress gets induced in the oxide layer and because of which cracks are formed in the titanium oxide layer. In addition to the mechanical stress, chemical damage can also take place to the oxide film due to highly acidic pH and less availability of scarcity oxygen ions at the electrode surface interface. These cracks are more prone to contribute as pitting corrosion sites. Electric field intensity is also very strong near these openings which results in the higher concentration of chloride ions at these highly charged specific areas. With high reactivity of chloride ions, they can penetrate titanium dioxide layer easily to cause pitting. Simultaneously, repassivation process occurs, but in highly acidic aqueous environment it stays limited to few micrometers. By forming chloro-complexes, tubular shapes are formed under the action of applied electric field. But, due highly dynamic reaction kinetics and mechanical stress plays crucial role in the releasing of nanotubes bundles. This explanation clearly shows the complexity of synthesizing TiO₂ nanotubes by rapid breakdown anodization.

3.5 <u>Overview of TiO₂ nanotubes synthesis by electrochemical anodization process:</u>

In comparison with RBA, the electrochemical anodization is the well-established and wellunderstood method to synthesize uniform arrays of the TiO₂ nanotubes on titanium substrates. The reaction kinetics of the electrochemical anodization method are completely different than that of the RBA method. In electrochemical anodization process, various TiO₂ nanotubes morphologies can be achieved by tuning its process parameters. Applied potential regulates the electric field strength and hence the migration of ions, which eventually affects the diameter of TiO₂ nanotubes. Electrochemical anodization in organic electrolytes follows the simultaneous field assisted oxidation and field assisted dissolution (50). The process kinetics are quite steady. So, smoother nanotubes walls and uniform structure of nanotubes can be achieved. In aqueous electrolytes, the dissolution rate of nanotubes is higher than that of its oxidation, so the overall length of nanotubes remains short (4-5 μ m). Also, one can observe the ripples on the walls of the nanotubes as the oxide formation and dissolution process is not continuous (75). Water content in the electrolyte and oxygen evolution at anode influences the formation of irregular nanotubes and ripples on the walls of the nanotubes due to the stacking of oxide rings (76). Anodization time controls the length of the nanotubes in the organic electrolytes, but day-long anodization time usually produces overdissolution of nanotubes in some areas. Fluoride ions concentration in the electrolytes is very crucial factor in the electrolytes. It should be low (0.2wt% - 0.5 wt%), good enough to promote nanotubular growth with optimum dissolution rate (77). Fluoride ions (F⁻) migration rate in the oxide film is twice than that of O_2^- ions, hence if the concentration is high more F⁻ ions will be found in the metal/metal-oxide interface which ultimately lead to the delamination of nanotubes (50). Higher concentration of fluoride ions forms stable complexes, $(TiF_6)^{2-}$ which also reduces dissolution rate of the oxide. Temperature of the electrolyte in organic electrolyte affects its viscosity and hence the flow of ions (78). At higher temperature, larger diameter nanotubes can be synthesized as the flow of F⁻ ions gets enhanced which promotes more dissolution of TiO₂.

Sr. No.	Aspects	Electrochemical anodization method	Rapid breakdown anodization method
01	Applied voltage	Sweeping: - Controls the diameter of nanotubes	Stepping: - Controls the number of nucleation sites on Ti foil
02	Electrolyte	Organic or aqueous: - Mainly with fluoride ions	Aqueous: - with chloride, bromide or perchlorate ions
03	Process mechanism	Plastic flow mechanism and steady in organic electrolyte	Very intense and breakdown events occur (pitting corrosion: in specific areas of foil)
04	Synthesized TiO ₂ nanotubes	Uniform nanotubes arrays can be formed on the Ti substrate	Non-uniform nanotubes bundles can be formed in powdered form
05	Time	With longer process time, larger nanotubes length can be obtained.	Process time doesn't control the nanotubes morphology. Fastest synthesis of TiO_2 nanotubes powder with large quantity can be achieved.

TABLE 03 - Comparison: Electrochemical anodization method and rapid breakdown anodiz	zation
method	

4. TiO2 NANOTUBES SYNTHESIS BY HYDROTHERMAL METHOD

4.1 <u>Overview</u>:

Kasuga is considered as the pioneer who synthesized the TiO₂ nanotubes by hydrothermal method in 1999 (79) (80). In hydrothermal process, the solvents containing precursors are applied to the critical temperature under autogenous pressure to perform the desired chemical reaction in the enclosed entity (80). When the water is used as solvent, the process is called hydrothermal. While if any organic solvent is used, the process is termed as solvothermal. For powders synthesis, constant temperature is applied in order to achieve recrystallization. Whereas if temperature gradient is applied over the specific period of time formation of larger crystals can be achieved from the reaction contents (80). TiO₂ nanotubes synthesized by hydrothermal method have various advantages, such as cheap production cost, high yield, mass synthesis, simple setup and individual nanotubes having high specific surface area and surface energy (81). The key limitation of this method is the prolonged process duration.

This section includes the primary understanding of hydrothermal process considering critical vapor temperature, pressure-temperature diagram depending on the filling factor and the solubility-molarity relation. Also, peeling-scrolling mechanism of TiO₂ nanotubes synthesis via hydrothermal process is included. Additionally, various parameters governing the hydrothermal process are briefly explained.

4.2 Hydrothermal process understanding:

In this section, critical aspects of hydrothermal process are briefly elaborated in order to gain some basic understanding of the process.

4.2.1 Process description:

In hydrothermal process, sealed reactor as known as 'autoclave reactor' is used. This autoclave contains a cylindrical Teflon liner in order to protect autoclave body from highly corrosive and reactive solvents which are held at high temperatures and pressures (82). In hydrothermal process, usually the temperature is kept above the boiling point of water. Precursors of required final product are added to induce the recrystallization or solute molecules are used to achieve the nucleation of crystals of desired sizes. The volume of solvent inside the autoclave reactor, that is, the filling fraction determines the pressure intensity. The duration of hydrothermal process quite often is very long like 6 hours, 24 hours, 48 hours or so on. Certain pretreatments in order to promote solute and solvent interactions have proven to be very effective to alter or control the morphology of final product after hydrothermal treatment. Also, post-hydrothermal treatments like acid rinsing contributes to obtain the desired morphology of the products by replacing certain unwanted ions. Post-hydrothermal process heat treatment is preferred to perform inside oven instead of furnace.

4.2.2 <u>Pressure-Temperature diagram in relation with volume (filling fraction):</u>

The filling fraction of the solvent volume occupied inside an autoclave reactor is the critical factor for maintaining pressure based on the temperature conditions.

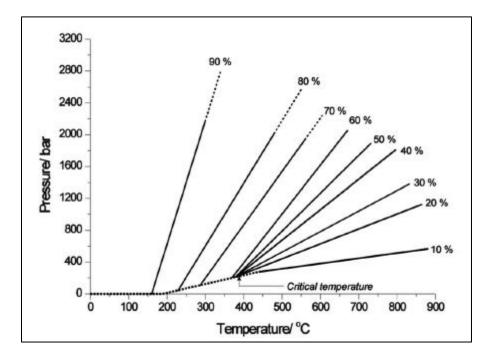


Figure 18 – Water pressure-temperature dependence of different autoclave filling fractions (84)

Critical temperature is the temperature at which both liquid and gaseous phases coexist. They possess equal density and hence new fluid is formed which is not completely water or not completely gaseous (85). For water this critical point exists on pressure-temperature curve at 374°C and at 22.5 MPa (225 bar) (83) (84). The dielectric constant of water is significantly decreased on which we will have more insights in the following sections. Due to extremely reduced dielectric constant at critical point, water behaves as the non-polar solvent as a result of which non-polar species can become more soluble (84).

In the above illustrative figure, if we consider volume fraction filled at 80%, the fluid state same as that at critical temperature point can be achieved even at low temperature of 245°C (85). Due to filled autoclave reactor container volume, saturated vapor pressure increases significantly. By increasing the temperature further more than 245°C will increase the pressure expressively.

4.2.3 <u>Role of mineralizer (catalyst)</u>:

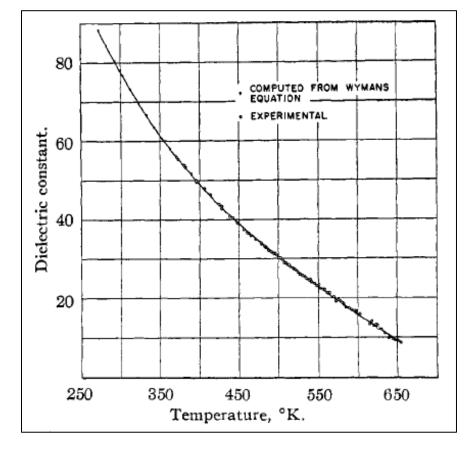
Mineralizer in hydrothermal process plays a crucial part to improve the solubility of the precursors. When even at higher temperatures water cannot provide required solubility of reagents, mineralizer forms complexes via ionic bonds which helps in solubilization of precursors and expedite the process (86). Commonly used mineralizers are strong bases like NaOH or KOH. Mineralizer mainly increases the reaction conversion rate and increases the solubility of metal oxides at higher pH values (86) (87).

In the case of TiO₂ as precursor and use of NaOH as mineralizer, hydroxyl ions increase the pH of the water solvent. TiO₂ rutile polymorph's solubility increases significantly at pH 10.5 in the heating range above 100°C (83). Na⁺ ions also plays important role by forming complexes with metal oxides and are responsible for the stability of dissolved metal oxide cations at higher temperatures during hydrothermal process (86).

4.2.4 <u>Factors governing solubility of metal oxides in water:</u>

Critical factors governing solubility of metal oxides in water under hydrothermal conditions are dielectric constant and pH of the water.

Dielectric constant of water is a physical property which signifies the intermolecular and interatomic attractions (88). It is defined as solvent's efficiency of separating electrolyte species into ions (88). The dielectric constant of water at room temperature is 78 while at supercritical conditions it drops below 10 which also promotes nucleation growth of crystals as water solubility decreases (82).



The relation of dielectric constant of water with respect to temperature is as follows:

Figure 19 – Water dielectric constant at variation in temperature (89).

The main reason for decrease in the dielectric constant with respect to increased temperature is the breaking of hydrogen bonding of water molecules and as a result solubility of solution species also decreases in heated water temperatures.

Additionally, water solvent pH is also a critical factor that governs solubility of metal oxides. The molarity of strong base like NaOH drives the pH of the water solvent. Hence it should be in the optimum range. Masturah et. al. described the study of the effect of the different molarities of NaOH on the synthesis of TiO_2 nanotubes (90). According to their studies, hydrothermal TiO_2 nanotubes can retain tube like structure with highest yield in 10 M NaOH solution, eventually if

this molarity has increased, it resulted in the rupture of nanotubular morphology and the decreased molarity of NaOH doesn't support the transformation into nanotubular shape.

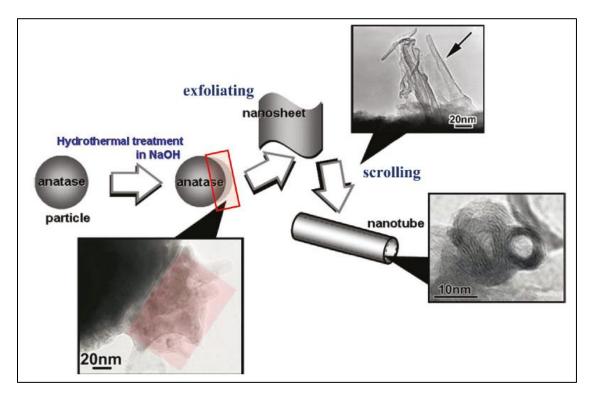
4.3 Formation mechanism of hydrothermal synthesis of TiO₂ nanotubes:

There are still controversial views about the actual mechanism of hydrothermal synthesis of TiO_2 nanotubes. According to Kasuga et. al., after hydrothermal synthesis of TiO_2 nanotubes, acid rinsing is the critical step which converts two dimensional hydrated titanate nanosheets into nanotubular shape (91). While Srimala et. al. carried out the study which shows the individual nanotubes morphology is obtained during hydrothermal synthesis itself and post-synthesis acid treatment is mainly responsible for the exchange of Na⁺ ions by H⁺ ions (92). This section includes the peeling-scrolling mechanism of TiO₂ nanotubes hydrothermal synthesis.

The reactions taking place in the hydrothermal process are as follows (93) (94):

(I) Dissolution of TiO₂ precursor: $TiO_{2pr} + 2NaOH \longrightarrow 2Na^{+} + TiO_{3}^{2-} + H_{2}O$ (10) (II) Dissolution and crystallization of nanosheets: $2Na^{+} + TiO_{3}^{2-} \longrightarrow (Na_{2}TiO_{3})_{nanosheet}$ (11) (III) Curving of nanosheets: $2Na^{+} + Ti_{3}^{2-} + (Na_{2}TiO_{3})_{nanosheet} \longrightarrow (Na_{2}TiO_{3})_{nanotubes}$ (12) (IV) Washing of nanotubes: H^{+} (Na TiO) = t 2UO = t 2UO = t 2 NaOH (12)

 $(Na_{2}TiO_{3})_{nanosheet} + 2H_{2}O \longrightarrow (H_{2}TiO_{3})_{nanotubes} + 2 NaOH$ (13)



Peeling and scrolling mechanism of hydrothermal synthesis of TiO₂ nanotubes:

Figure 20 – Schematic of exfoliation and scrolling mechanism (95)

In brief, following are the four main stages of hydrothermal TiO₂ nanotubes synthesis (91):

- dissolution of TiO₂ precursor and breaking of Ti-O-Ti bonds in the concentrated alkaline solution
- 2. formation and growth of layered nanosheets of sodium titanate
- 3. exfoliation of nanosheets
- 4. growing of nanosheets with tendency to curl and as a result formation of nanotubes

Over the period, various reasons are proposed as the driving force for the curling of nanosheets into these nanotubes. Single layer hydrated titanate ($H_2Ti_3O_7$) structures possess the asymmetric distribution of hydrogen atoms on adjacent sides of the layer and this deficiency of hydrogen atoms on one side creates the surface tension (91). This surface tension increases in order to scroll

the nanosheet into nanotube. Another proposed reason for this driving force is the mechanical stress getting generated during dissolution of TiO₂ precursor and crystallization process (91).

4.4 Hydrothermal synthesis of TiO₂ nanotubes process control parameters:

4.4.1 <u>Pretreatment – Ultrasonication</u>:

Ultrasonication is very simple but crucial step in the hydrothermal synthesis of TiO_2 nanotubes. Ultrasonication improves dispersion of nanoparticles inside the solution and breaks intermolecular interactions between TiO_2 precursors and highly concentrated alkaline molecules (96). This improves the homogeneous dispersion of precursor particles and ultimately helps in achieving longer length nanotubes as compared with non-ultrasonicated solution during hydrothermal process.

4.4.2 Alkali concentration:

Alkali concentration is the responsible factor for the dissolution of TiO₂ precursor. Alkali products are basically the catalyst or mineralizer which accelerate the reaction rate under hydrothermal conditions and also control the exfoliation rates and hence crucial to maintain nanotubular morphology (91). If this concentration of NaOH is as low as 5M or as high as 15M in the solution, it affects the process adversely due to deficiency or excess number of ions by which destroying the nanotubular shape.

4.4.3 Precursor:

 TiO_2 precursor used for the hydrothermal process is a critical parameter. Different crystalline types and different sizes of precursors affect the final synthesized nanotubular product. Precursor is responsible for the thermal and structural stability of as-synthesized TiO_2 nanotubes (91). If the precursor is in crystalline form, single layer of nanosheet can be delaminated from it

which eventually is accountable for the nanotubular morphology. Hence, anatase or P25 TiO_2 precursors are effective to obtain desired nanotubular shapes. If amorphous TiO2 is used as precursor, needle-like nanocrystals are formed instead of crystalline (91).

4.4.4 Temperature:

To achieve the high yield of synthesized TiO_2 nanotubes, the temperature of the hydrothermal process should be between the range of $110^{\circ}C - 150^{\circ}C$ (97). Hydrothermal process temperature controls the nucleation and crystal growth of TiO_2 nanotubes. It is the main constituent for the breaking of Ti-O-Ti bonds by Na+ by forming Ti-O-Na and Ti-OH bonds (91). Temperature is the important parameter which can synthesize longer length and crystalline nanotubes. By increasing the temperature more than 180°C, nanorods are synthesized instead of nanotubes (91).

4.4.5 Process time:

Hydrothermal process time is responsible for the yield and the morphology as-synthesized TiO₂ nanotubes. To achieve maximum yield of nanotubes, process durations of 24 hours or more are usually preferred. After 3 hours the layered structures are developed from the spherical TiO₂ precursors, which indicates the breaking of Ti-O-Ti bonds into Ti-O-Na and Ti-OH bonds (92).

4.4.6 Post-treatment- acid washing:

Acid washing stage has an influence on the final elemental composition and the surface area of the as-synthesized TiO₂ nanotubes (96). While rinsing with the hydrochloric acid, Na⁺ ions are replaced with H⁺ ions. Additionally, the molarity of hydrochloric acid while washing stage is extremely vital, as concentration more than 2M can destroy the nanotubular morphology of TiO₂ nanotubes (98).

4.5 <u>Applications of TiO₂ nanotubes synthesized by hydrothermal method:</u>

By taking into the consideration, the advantages of individuality, high specific surface area of $350 \text{ m}^2/\text{g}$, bioinert properties, high yield; over the last decade the hydrothermal TiO₂ nanotubes are widely utilized for various applications such as photocatalysts, environmental purification, bone regeneration, photoinduced hydrophilicity, drug delivery and dye-sensitized solar batteries (96) (97).

5. PROJECT OBJECTIVES

The currently available arthroplasty surgeries yearly statistical data clearly postulates that the state of the art PMMA bone cements have limitations over sufficient mechanical strength and bioactivity properties. Hence, more efforts are required to find appropriate filler materials which can enhance mechanical strength and bioactivity without interrupting biocompatibility of PMMA bone cements.

This research work proposes that by using individual TiO₂ nanotubes and silver doped hydroxyapatite (Ag-HA) nanobelts as filler materials, PMMA bone cement composites can overcome aforementioned limitations. TiO₂ nanotubes are well-known for their biocompatibility, mechanical strength, drug loading capacity and radiopacity; while Ag-HA nanobelts can induce bioactivity and antibacterial properties to the PMMA bone cements. In this study, individual TiO₂ nanotubes are synthesized by hydrothermal method which has advantages over cost effective mass production and ease of synthesis. Ag-HA nanobelts are also synthesized by hydrothermal method which are used as-synthesized by other student for comparative study between two fillers. Additionally, TiO₂ nanotubes are synthesized by rapid breakdown anodization (RBA) method. Considering future scope for further development of PMMA bone cements, RBA synthesized TiO₂ nanotubes will be utilized as they have unique advantage of cost effective fastest production rate.

In general, the project objectives for comparative study between PMMA bone cement composite samples with individual TiO₂ nanotubes and Ag-HA nanobelts as fillers can be summarized as mentioned below.

1. To synthesize nano-filler materials analyzed with various characterization techniques like transmission electron microscopy (TEM), field emission scanning electron microscopy (FESEM), energy dispersion X-ray spectroscopy (EDS) and X-ray diffraction (XRD).

- 2. To achieve homogeneity in PMMA bone cement composite samples with specific weight percent of filler material.
- 3. To evaluate cytotoxicity of PMMA composite samples with specific weight percent of filler materials by performing MTT cells viability assay.
- 4. To evaluate mechanical properties of PMMA bone cement composites at specific weight percent of fillers by assessing respective compressive strength and elastic modulus.
- 5. To assess antibacterial properties of PMMA composite samples incorporated with specific weight percent of fillers by disc diffusion method.

6.1 Synthesis of TiO₂ nanotubes by rapid breakdown anodization (RBA) method:

6.1.1 Materials:

Titanium foil (0.25 mm thickness, 99.7% trace metals basis) was purchased from Sigma-Aldrich. For electrolyte species perchloric acid (HClO₄) (70%, 99.999% trace metals basis) was procured from Aldrich. Deionized (DI) water with 18 megaohm resistivity was used for anodization process.

6.1.2 Methods:

The protocol as mentioned by Fahim et. al. was followed to synthesize TiO_2 nanotubes by rapid breakdown anodization process (49). Titanium foil of 35 mm in length and 25 mm in width was used as anode. Prior to anodization, titanium foil was rinsed and ultrasonicated successively by ethanol and DI water for 10 minutes each. Pt foil with same size as anode was used as counter electrode. The distance between the electrodes was set to 20 mm. 0.1 M HClO₄ was used as an electrolyte. Anodization was carried out by applying 20 V stepping voltage for 30 minutes. During the anodization process, magnetic stirrer speed was constant at 400 rpm. Current - time transients were observed from Agilent E3634A DC power supply. By the end of 30 minutes of anodization process, the electrolyte was turned bulky with TiO₂ nanotubes powder which was formed from titanium foil. Afterwards, as-synthesized TiO2 nanotubes powder was rinsed by centrifugation at 8000 rpm and dried in vacuum oven at 80°C for 24 hours.

These synthesized TiO₂ nanotubes were characterized by using field emission scanning electron microscopy (FESEM) and transmission electron microscopy (TEM). FESEM images of RBA synthesized TiO₂ nanotubes were obtained at 2.5 kV accelerating voltage by using JEOL JSM-6320F FESEM device. Prior to imaging TiO₂ nanotubes powder was coated with 7 nm gold

particles. For TEM imaging, samples were prepared by mixing 0.5 mg of nanotubes powder in 1 ml of ethanol and ultrasonicated for 3 minutes. 2 μ L of dispersed solution was taken on Lacey carbon TEM grid. TEM images were obtained on JEOL 3010 at accelerating voltage of 300 kV.

6.2 <u>TiO₂ nanotubes synthesis by hydrothermal method:</u>

6.2.1 Materials:

Anatase titania powder (Titanium (IV) oxide, anatase nanopowder < 25 nm particle size, 99.7 % trace metals basis) and Hydrochloric acid (HCl) (37%, reagent grade) were purchased from Sigma-Aldrich. Sodium hydroxide (NaOH) in the pellets form was procured from Fisher Scientific. Deionized (DI) water with 18 megaohm resistivity was used for anodization process.

6.2.2 Method:

The protocol as specified by Tsai et. al. was followed to synthesize individual multiwalled TiO₂ nanotubes by hydrothermal method (99). TiO₂ anatase crystalline powder of less than 25 nm particle size was used as precursor. The 1.5 g of precursor powder was mixed with 50 ml of 10 M NaOH solution by stirring for 30 minutes followed by 30 minutes of ultrasonication. This pretreated solution was added to the 80 ml of Teflon lined autoclave reactor. Thermal treatment is carried out at 150°C in oven for 24 hours. Followed to the heat treatment, the supernatant solution was slowly decanted and synthesized TiO₂ nanotubes powder was post-treated by following a protocol as mentioned by Mozia et. al. (100). Primarily, as synthesized TiO₂ nanotubes powder was rinsed with 500 ml of 0.1 M HCl solution with 20 minutes of stirring in a beaker and 40 minutes of additional without stirring treatment. Then TiO₂ nanotubes powder precipitate was recovered by centrifugation and again mixed with newly prepared 500 ml of 0.1 M HCl solution under 20 minutes of stirring and 80 minutes steady treatment. Final precipitate was rinsed with DI

water again and again till achieving pH of the final solution around 6. Subsequently, final posttreated powder precipitate was dried in vacuum oven at 80°C for 24 hours. To study the anatase crystalline form of dried amorphous powder sample was calcined at 400°C for 5 hours (101).

For characterization, transmission electron microscope (TEM) imaging was performed. TEM samples were prepared by mixing 0.5 mg of nanotubes powder in 1 ml of ethanol and ultrasonicated for 3 minutes. 2 μ L of dispersed solution was taken on Lacey carbon TEM grid. TEM images were obtained on JEOL 3010 at accelerating voltage of 300 kV. X-ray diffraction patterns of as-synthesized TiO₂ nanotubes powder and calcined TiO₂ nanotubes powder were obtained by using Bruker D8 Discover X-ray diffractometer by using CuK_a radiation ($\lambda = 1.54$ A^o) in the 20 range from 5° to 70°.

6.3 Ag-HA nanobelts synthesis by hydrothermal method:

6.3.1 Materials:

Silver nitrate (AgNO₃) (99.9999% trace metals basis), Urea (NH₂CONH₂) (reagent grade, 98%), Nitric acid (HNO₃) (ACS reagent, \geq 90%), Ammonium phosphate monobasic (NH₄H₂PO₄) (ACS reagent, \geq 98%) and Calcium nitrate tetrahydrate (Ca(NO₃)₂.4H₂O) (BioXtra, \geq 99%) were purchased from Sigma-Aldrich. Deionized (DI) water with 18 megaohm resistivity was used.

6.3.2 <u>Method:</u>

Hydrothermal precipitation method was used to synthesize Ag-HA nanobelts (102). To start with, the aqueous solutions of calcium nitrate tetrahydrate and ammonium phosphate monobasic with were mixed under magnetic stirring (Ca/P molar ratio of 1.67). Then 1 M urea was added to the above mixture.

The initial pH of the solution was adjusted to 3.5 by using 0.5 M nitric acid. After adding AgNO₃ powders in required ratio, the solution was transferred into 80 ml Teflon-lined autoclave reactor, followed by simultaneous heat-treatment at 160°C for 6 h with the help of oven. Then the reaction product was rinsed thoroughly with deionized water and anhydrous ethanol, and dried at 80°C for 24 hours.

Field emission scanning electron microscopy (FESEM) images of Ag-HA nanobelts were obtained at 15 kV accelerating voltage by using JEOL JSM-6320F FESEM device.

6.4 MTT cells viability assay:

6.4.1 <u>Materials:</u>

For bone cement composite samples preparation, polymethylmethacrylate (PMMA) (inherent viscosity ~1.25 dL/g (lit.), crystalline) polymer powder and methyl methacrylate (MMA) liquid monomer were procured from Aldrich.

For cell culture experiments, Dulbecco's modified Eagle medium (DMEM; Gibco), dimethyl sulfoxide (DMSO, Fisher Chemical), fetal bovine serum (FBS; Gibco), Thiazolyl Blue Tetrazolium Bromide (98%, MTT; Sigma), Phosphate Buffered Saline (PBS; Sigma), 0.05% Trypsin-EDTA (1X) (gibco) and penicillin streptomycin (Penstrep, gibco) were purchased.

6.4.2 Methods:

PMMA bone cement composite cylindrical samples of 6 mm diameter X 3 mm height were prepared by mixing PMMA polymer and MMA monomer in 2:1 g/ml powder to liquid ratio with the help of transparent poly acrylic mould and plunger. Control PMMA sample (CP1) (PMMA + MMA), PMMA – hydrothermal TiO₂ nanotubes (PT10) (10 wt% TiO₂ + PMMA + MMA) and PMMA – Ag-HA nanobelts (PH10) (10 wt% Ag-HA + PMMA + MMA) cylindrical samples were prepared in triplicates for cell culture experiments.

MTT solution was prepared by diluting MTT in PBS with a concentration of 5 mg/ml. Fibroblasts cells (3T3-J2) were cultured in Dulbecco's modified Eagle medium (DMEM) supplemented with 10% fetal bovine serum (FBS) and 1% penicillin streptomycin (Penstrep). The 3T3-J2 cells were maintained under a humidified environment of 5% CO₂ at 37°C till obtaining 80-90% confluency. Cell viability was evaluated by MTT reduction assay (103). Aforementioned PMMA bone cement composite cylindrical samples were sterilized under UV overnight and placed in 96-well plate as in triplicates. Then, 3T3-J2 cells were seeded in 96-well plate including control sample by maintaining the concentration as 10000 cells/well and incubated for 24 hours. Thereafter, 10 volume% MTT solution was added to each well and well-plate was incubated for 4 hours at 37 °C in the dark. Subsequently, equal volume as cell seeded media, DMSO was added to each well to solubilize formazan salts and well plate was ultrasonicated at room temperature in the dark for 20 minutes. Finally, an absorption was assessed by a microplate reader (SynergyTM H1, BioTek) at 570 nm wavelength as cells viability is directly proportional to the absorption value.

6.5 <u>Compression test:</u>

6.5.1 Materials:

For bone cement composite samples preparation, polymethylmethacrylate (PMMA) (inherent viscosity ~1.25 dL/g (lit.), crystalline) polymer powder and methyl methacrylate (MMA) liquid monomer were procured from Aldrich. TiO₂ hydrothermal nanotubes and Ag-HA nanobelts were synthesized as described before.

6.5.2 Method:

According ISO5833 standard, PMMA bone cement composite cylindrical samples of 6 mm diameter X 12 mm height were prepared by mixing PMMA polymer and MMA monomer in 2:1 g/ml powder to liquid ratio with the help of transparent poly acrylic mould and plunger. PMMA – hydrothermal TiO₂ nanotubes (PT2.5) (2.5 wt% TiO₂ + PMMA + MMA) and (PH1.25) (1.25 wt% Ag-HA + PMMA + MMA) cylindrical samples were prepared in triplicates for compression test comparative study between the fillers.

Compression test was carried out on INSTRON – 8500R universal testing machine. The crosshead speed was 0.1 inch/min. Force Vs. displacement graphs were recorded in order to find modulus of elasticity along with ultimate compressive strength.

6.6 In-vitro antibacterial test:

6.6.1 Materials:

Escherichia coli (E.coli) (ATCC® 29425) Gram-negative strain bacteria, LB Agar Miller (Molecular genetics powder, Fisher Bioreagents), LB Broth (Lennox) – EzMixTM powder microbial growth medium (Sigma Aldrich), Molecular Biology Grade Water (Corning) and 100 mm X 15 mm sterile polystyrene petri dish (Fisherbrand) were used to perform antibacterial inhibition zone test.

6.6.2 Method:

For in-vitro antibacterial inhibition zone test, compressed disc samples of PMMA, hydrothermal TiO₂ nanotubes and Ag-HA nanobelts powders of 15 mm diameter were prepared by compressing 200 mg powders of each sample with the help of 24T hydraulic press by maintaining applied pressure at 2000 psi.

Antibacterial properties of PMMA, Ag-HA nanobelts and hydrothermal TiO₂ nanotubes were evaluated by disc diffusion method (104). LB Broth medium was prepared as per manufacturer's instructions and sterilized at 260°F with wet autoclave cycle. The *Escherichia coli* (*E. coli*) bacterial stock solution was prepared by incorporating *E. coli* Gram negative strain in sterilized LB broth medium and incubating overnight at 37°C under shaking. LB Agar plates were prepared by maintaining the concentration 37 g/L (LB Agar powder to LB Broth medium ratio). 100 μ L of bacteria cultured stock solution was inoculated onto each agar plate. Then compressed disc samples were placed on seeded agar plates. Then agar plates were incubated at 37°C for 24 hours and their inhibition zones were compared by measuring their respective diameters of inhibition zones.

7. RESULTS AND DISCUSSION

7.1 Characterization of TiO₂ nanotubes synthesized by RBA:

For studying the morphology of TiO₂ nanotubes bundles synthesized by RBA, FESEM images were observed (refer Fig:16 (a) and (b)) FESEM images clearly indicates that the average nanotubes bundles length was 6.93 μ m and that the width was 1.85 μ m. FESEM images confirm nanotubular morphology of individual TiO₂ nanotubes stacked in the bundles, but the assynthesized nanotubular bundles lack uniformity in overall dimensions.

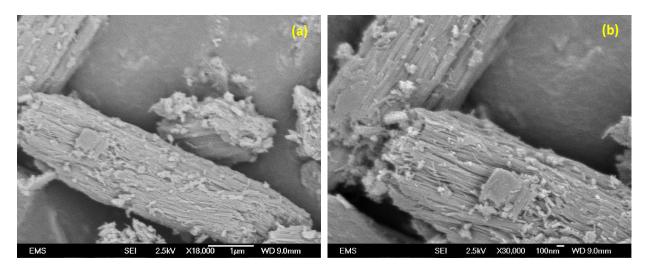


Figure 21 – FESEM images of TiO2 nanotubes synthesized by RBA

To study the internal and external diameters of individual as-synthesized RBA TiO_2 nanotubes along with wall thickness, TEM images are observed (refer Fig:17 (a) and (b)). TEM images clearly show the internal and external diameters of high aspect ratio nanotubes is maintained throughout the morphology. The average internal diameter of as-synthesized TiO_2 nanotubes stacked in a bundle is approximately 7.6 nm and that the external diameter is 18.5 nm which also implies wall thickness as 5.45 nm.

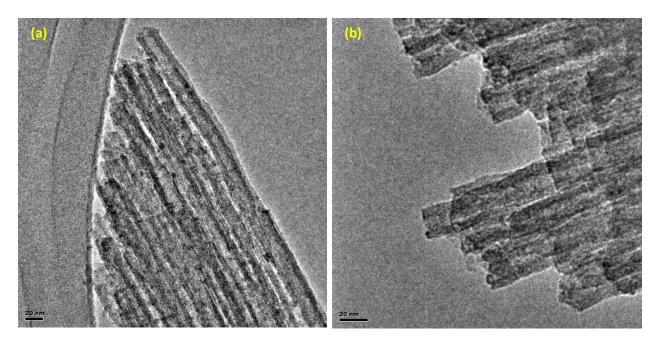


Figure 22 – TEM images of TiO₂ nanotubes synthesized by RBA

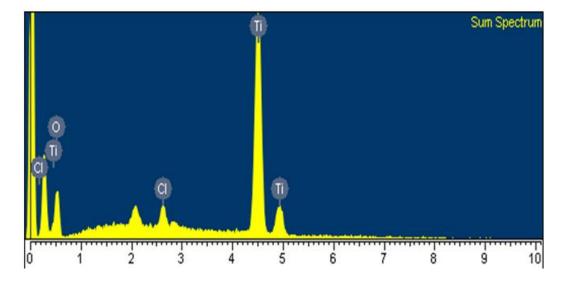


Figure 23 – Energy dispersion X-ray spectroscopy (EDS) spectrum of RBA TiO₂ nanotubes

7.2 <u>Characterization of TiO₂ nanotubes synthesized by hydrothermal method:</u>

Transmission electron microscope (TEM) images clearly confirm the maintained individuality of synthesized hydrothermal TiO_2 nanotubes (refer Fig:18 (a) and (b)). TEM results indicate that the average length of individual TiO2 nanotubes is around 99.5 nm, whereas their

average internal diameter is 4.25 nm and that the external diameter is around 10.25 nm. Additionally, these results also confirm the multiple uneven number of nanotubes walls on each side of individual nanotubes with approximate intermediate walls spacing of 0.78 nm which also supports the findings of Yuan and Su (97).

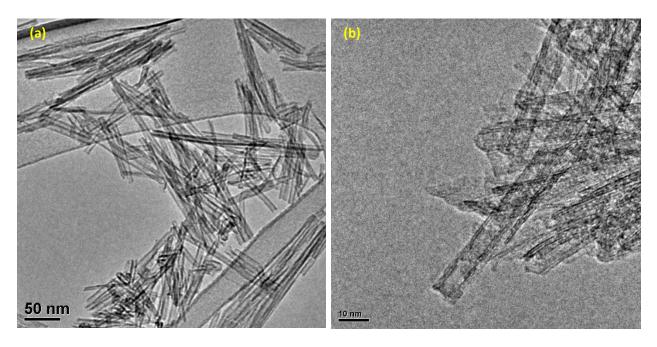


Figure 24 – TEM images of TiO₂ nanotubes synthesized by hydrothermal method

In order to study the difference between as-synthesized amorphous TiO2 nanotubes and after 5 hours at 400oC calcination anatase TiO2 nanotubes XRD patterns are compared. XRD results are in accordance with Jiang et. al. confirming the diffraction peaks at specific 2 θ angles as per hydrated titanate and anatase structure (101). The diffraction peaks of 2 θ at ~10°, 24.5° and 48.5° corresponds to (200), (110) and (020) planes respectively which are indexed to H₂Ti₃O₇.nH₂O (hydrated trititanate) phase (101) (105). Also, the diffraction peaks of 2 θ at 25.4°, 37.8°, 48°, 53.8° and 55.1° confirm the anatase crystal structure which is acquired after calcination.

Increasing the calcination temperature weakened the (200) peak, which also assures transformation to crystalline phase.

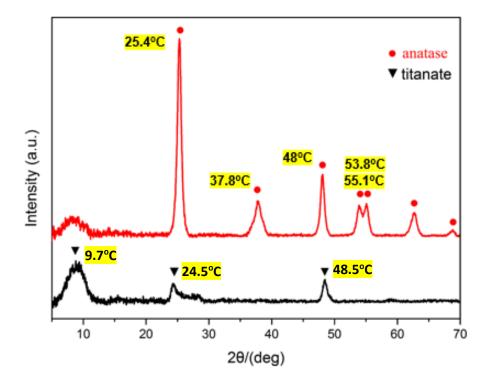


Figure 25 – XRD pattern of as-synthesized and calcined (400°C for 5 hours) hydrothermal $\rm TiO_2$ nanotubes

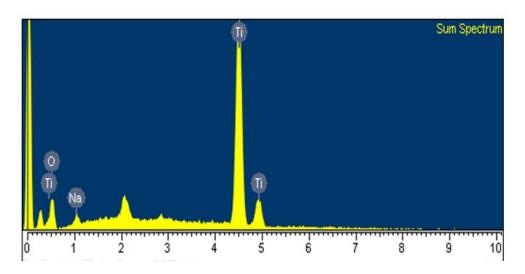


Figure 26 – Energy dispersion X-ray spectroscopy (EDS) spectrum of hydrothermal TiO₂ nanotubes

7.3 Characterization of Ag-HA nanobelts:

FESEM image of Ag-HA nanobelts shows that the average length of as-synthesized nanobelts is approximately 180 μ m. An average aspect ratio of these Ag-HA nanobelts is between 70 – 90. (refer Figure 27)

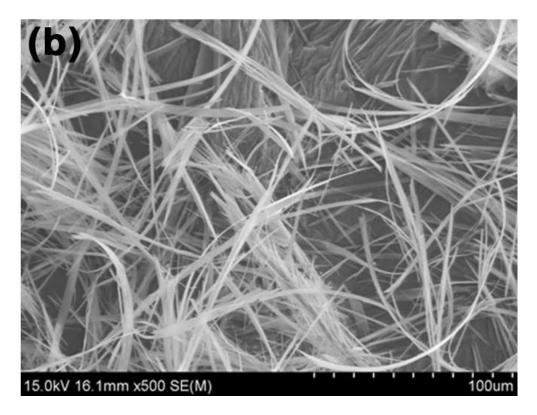


Figure 27 – FESEM image of Ag-HA nanobelts (102)

7.4 Cytotoxicity study of PMMA bone cement composites by MTT assay:

MTT assay absorbance results indicate the comparative study between control sample (cells + media), Pure PMMA sample, PMMA incorporated with 10wt% TiO₂ nanotubes and PMMA incorporated with 10wt% Ag-HA nanobelts. Results are analyzed by using one-way ANOVA and Post-hoc t-Test. In comparative study, p value < 0.05 is considered to be statistically significant. For pair-wise comparison between groups Post-hoc t-Test is carried out. (* - indicates the significance in variation in data between Control sample and all other PMMA groups, while # - indicates the significance in variation in data between pure PMMA and PMMA incorporated with 10wt% TiO₂ and 10wt% Ag-HA groups).

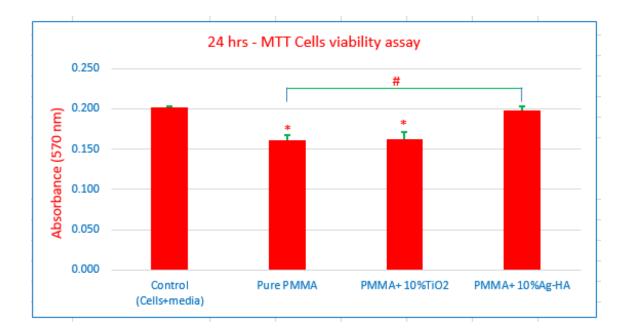


Figure 28 – MTT assay absorbance results (* - one-way ANOVA between control sample and PMMA groups, # - one-way ANOVA between Pure PMMA and other PMMA groups, p < 0.05)

Sr. No.	Sample specification	% Cells viability
01	Pure PMMA	80.19 %
02	PMMA + 10wt% TiO2	80.69 %
03	PMMA + 10wt% Ag-HA	98.51 %

TABLE 04 - % Cells viability based on MTT absorption results

TABLE:04 shows the % cells viability with respect to the control sample. MTT assay results clearly indicate that the cells viability has increased with the incorporation of Ag-HA nanobelts in comparison with pure PMMA which also indicates induced bioactivity. 10wt% Ag-HA nanobelts integration has increased cells proliferation by 18.32 % in comparison with pure PMMA bone cement sample. Ag concentration in HA nanobelts didn't induce cytotoxicity in the PMMA bone cement which also confirms its percentage is within allowable limits. And at the same time, cells viability for 10wt% TiO₂ incorporated PMMA bone cement did not induce any cytotoxicity assuring their biocompatibility nature.

7.5 <u>Compression test:</u>

To evaluate the effect of incorporation of filler materials TiO_2 nanotubes and Ag-HA nanobelts in the PMMA bone cement matrix, both the fillers are compared in addition at specific weight percent to the pure PMMA matrix.

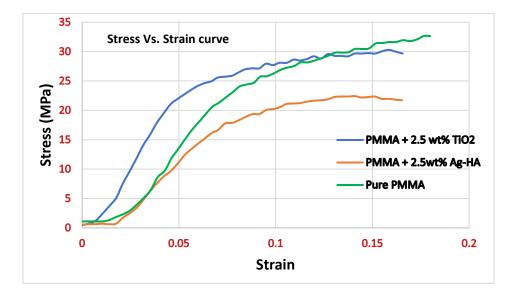


Figure 29 – Stress Vs. Strain curve: comparison between Pure PMMA, PMMA with 2.5wt% TiO₂ nanotubes as filler and PMMA with 2.5 wt% Ag-HA nanobelts as filler

Sr. No.	PMMA Composite	Young's modulus (E)
01	Pure PMMA	425.06 MPa
02	PMMA + 2.5 wt% TiO ₂ nanotubes	561.37 MPa
03	PMMA + 2.5 wt% Ag-HA nanobelts	353.73 MPa

TABLE 05 – PMMA composite Young's modulus

Preliminary compression test results of PMMA bone cement composites reinforced with TiO₂ nanotubes and Ag-HA nanobelts at 2.5 wt% indicates that the TiO₂ nanotubes have increased the compressive strength of PMMA bone cement composites in comparison with that of Ag-HA nanobelts reinforcement. One of the main reason is associated with the nano-filler dispersion and hence better degree of homogeneity of TiO2 nanotubes in the PMMA matrix as that compared with Ag-HA nanobelts micro-filler. Fig:23 shows the stress-strain curve of bone cements with the reinforcement of TiO₂ nanotubes and Ag-HA nanobelts from which we can calculate Young's

modulus for respective compositions (refer TABLE:05). Fig:24 indicates the compressive strength of (PMMA + 2.5 wt% TiO₂ nanotubes) is 23.57% more than that of (PMMA + 2.5 wt% Ag-HA nanobelts). Eventually both the fillers have shown lower compressive strength than pure PMMA, which signifies the need to improve the samples preparation method with decreased filler content.

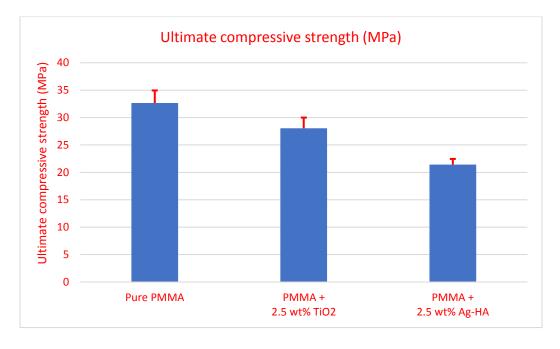


Figure 30 – Ultimate compressive strength (MPa)

According to the state of the art PMMA bone cements and ISO5833 standard, minimum required compressive strength is 70 MPa and that the Young's modulus is 2.1 GPa (28). In order to achieve the mechanical strength requirements of state of the art bone cements, sample preparation method needs to be altered. This existing experimental preliminary data doesn't fulfill this requirements, but it can confirm the effect of incorporation of filler materials at specific weight percent in the PMMA bone cement matrix by signifying the importance of individual TiO₂ nanotubes.

7.6 In-vitro antibacterial test:

PMMA doesn't have any antibacterial attributes and hence PMMA bone cements are always incorporated with antibiotics like gentamicin sulfate. To confirm the antibacterial activity of individual filler materials TiO₂ nanotubes and Ag-HA nanobelts, disc-diffusion method is used. Powder disc shaped pallets were prepared as mentioned in the methods section. To evaluate the antibacterial activity, zone of inhibition around the filler powder pallets are studied (refer Fig:25). As expected amorphous TiO₂ nanotubes don't have any zone of inhibition. Around Ag-HA nanobelts powder pallet clear zone of inhibition (19 mm diameter) can be seen, which also supports the objective and purpose of incorporating Ag doped HA nanobelts use as filler material in PMMA bone cement composite matrix. For this study, the concentration of Ag was maintained to its certain level, since the higher amount of Ag in the material can incorporate cytotoxicity along with anti-microbial effect (106). Ag ions kills bacteria by penetrating their membrane and failing nuclei functioning.

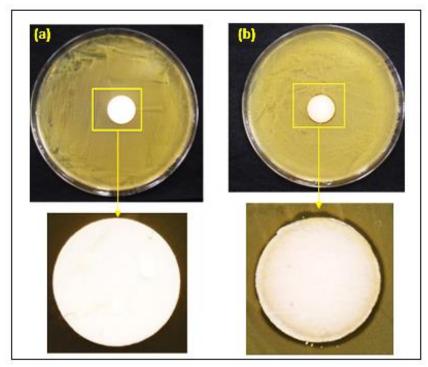


Figure 31 – Disc diffusion inhibition zone method (a) TiO₂ nanotubes powder pallet and (b) Ag-HA nanobelts powder pallet

8. CONCLUSIONS

The primary project goal of synthesis of PMMA bone cement composite nanofillers viz. hydrothermal individual TiO₂ nanotubes, RBA bundled TiO₂ nanotubes and Ag-HA nanobelts is successfully achieved and results are well-supported with various characterization techniques such as FESEM, TEM, EDS and XRD.

MTT cells viability assay results clearly shows the enhanced bioactivity with the incorporation of Ag-HA nanobelts as filler and subsequently proving biocompatibility with the incorporation of hydrothermal TiO₂ nanotubes as filler in the PMMA bone cement matrix which ultimately satisfied the research hypothesis of integrating respective fillers. With the incorporation of Ag-HA nanobelts at 10wt%, cells viability has increased by 17.32% as compared with the pure PMMA samples and with the incorporation of TiO₂ nanotubes at 10wt% cells viability remained the same indicating the absence of cytotoxicity. One-way ANOVA and post-hoc t-Test clearly confirms the statistical significance of the data.

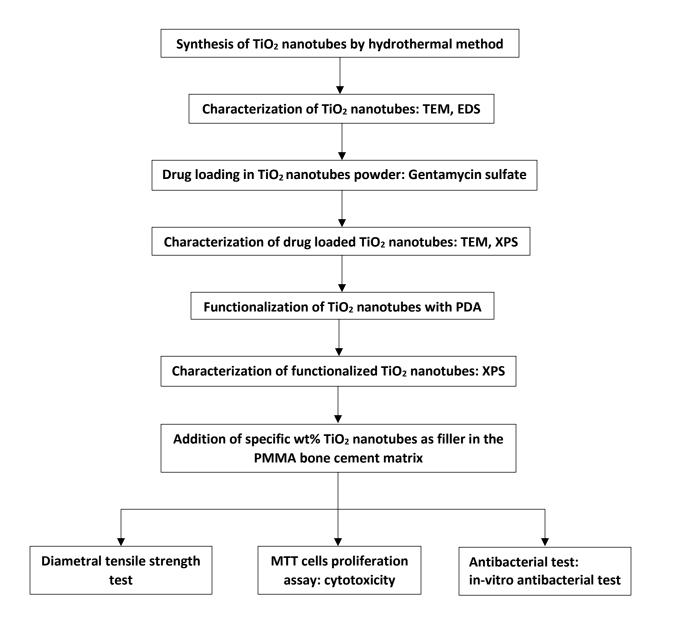
Mechanical compression test preliminary results clearly indicate that the compressive strength of PMMA bone cement composite has increased significantly with the reinforcement of TiO₂ nanotubes as that compared with the reinforcement of Ag-HA nanobelts. But, eventually currently prepared both nanofillers composite samples couldn't satisfy the minimum compression strength 70 MPa requirement of the state of the art PMMA bone cements. Hence, quality of the PMMA bone cement composite samples needs to be improved by altering the samples preparation method for further mechanical testing.

In-vitro antibacterial test results confirm the antibacterial activity of individual fillers. Ag-HA nanobelts pallet has shown the clear zone of inhibition while as expected for TiO₂ nanotubes pallet there is no zone of inhibition. Silver concentration of Ag-HA nanobelts is within optimum range which has induced anti-bacterial properties without displaying any cytotoxic effect. Also, further study is required for evaluating antibacterial effect with the incorporation of nanofillers at specific weight percent in the PMMA bone cement composite matrix. Hydrothermally synthesized TiO₂ nanotubes has excellent drug loading capacity due to their maximum surface area, which can be utilized to incorporate Gentamicin Sulfate antibiotic to enhance the antibacterial activity of the PMMA bone cement.

9. FUTUTRE SCOPE

The interfaces between bone-cement-implant are known as 3-weak links. The reasons for being weak links are mainly insufficient mechanical strength, lack of cells adhesion and proliferation and interfacial bacterial infection. This project work can be extended to overcome these challenges with incorporation of functionalized filler material in the PMMA bone cement matrix. Existing PMAM bone cements lack in the sufficient bioactivity and sufficient mechanical strength.

Individual TiO₂ nanotubes synthesized by hydrothermal method have numerous advantages. In the current study, TiO₂ nanotubes as a filler material has enhanced elastic modulus of PMMA bone cement. To provide antibacterial properties to these nanotubes, antibiotic drug can be loaded inside these nanotubes. Due to very high specific surface area (~ 370m²/g) and high surface energy drug loading capacity of hydrothermally synthesized TiO₂ nanotubes is very high. Drug loaded TiO₂ nanotubes can be functionalized with polydopamine (PDA) which has its various advantages in the biomedical field in the unique way. Polydopamine possesses amine group (-NH₂) which can replace hydroxyl group (-OH) of TiO₂ nanotubes which in terms can have chemical bonding. PDA also has been used in the biomedical field as an adhesive film layer and it also can enhance cells adhesion and proliferation. Besides PDA functionalized TiO₂ nanotubes can have individuality and better dispersion in the PMMA bone cement matrix which can improve mechanical properties of bone cement. Considering these advantages following study is proposed which is represented in the comprehensive way as follows:



CITED LITERATURE

- 1. Mousa, Weam F., Masahiko Kobayashi, Shuichi Shinzato, Masaki Kamimura, Masashi Neo, Satoru Yoshihara, and Takashi Nakamura. "Biological and mechanical properties of PMMA-based bioactive bone cements." *Biomaterials* 21, no. 21 (2000): 2137-2146.
- 2. Zhu, Xuesong, Xiaoqing Chen, Chunmao Chen, Genlin Wang, Yong Gu, Dechun Geng, Haiqing Mao, Zhiming Zhang, and Huilin Yang. "Evaluation of calcium phosphate and calcium sulfate as injectable bone cements in sheep vertebrae." *Clinical Spine Surgery* 25, no. 6 (2012): 333-337.
- 3. Malchau, Breusch, G. Garelick, and P. Herberts. "The well-cemented Total Hip Arthroplasty, Theory and Practice." (2005).
- 4. Turan, Ibrahim, Torsten Wredmark, and Li Felländer-Tsai. "Arthroscopic ankle arthrodesis in rheumatoid arthritis." *Clinical orthopaedics and related research* 320 (1995): 110-114.
- 5. Walker, Sue, Maryann Wood, and Jenny Nicol. *Mastering Medical Terminology-EBOOK PUB3/EPUB: Australia and New Zealand*. Elsevier Health Sciences, 2016.
- 6. Springer, Bryan D., and Caryn D. Etkin. "The American Joint Replacement Registry and Arthroplasty Today." *Arthroplasty Today* 2, no. 2 (2016): 43.
- 7. Abdel, Matthew P., and Craig J. Della Valle, eds. *Complications after Primary Total Hip Arthroplasty: A Comprehensive Clinical Guide*. Springer, 2017.
- 8. <u>https://www.arthritis-health.com/blog/cost-hip-replacement</u> (Accessed: November 3, 2017)
- 9. <u>https://commons.wikimedia.org/wiki/File:603_Anatomy_of_Long_Bone.jpg_</u>(Accessed: November 3, 2017)
- 10. <u>https://commons.wikimedia.org/wiki/File:Femur_-anterior_view2.png</u> (Accessed: November 3, 2017)
- 11. <u>http://www.innerbody.com/image_skelfov/skel25_new.html</u> (Accessed: November 3, 2017)
- 12. <u>http://study.com/academy/lesson/cancellous-bone-definition-structure-function.html</u> (Accessed: November 4, 2017)
- 13. <u>http://orthoinfo.aaos.org/topic.cfm?topic=a00377</u> (Accessed: November 6, 2017)
- 14. Derar, H., and M. Shahinpoor. "Recent patents and designs on hip replacement prostheses." *The open biomedical engineering journal* 9 (2015): 92.

- 15. <u>http://www.kneesandhips.net/operations/hip-replacement/cemented-hip-replacement/</u> (Accessed: November 6, 2017)
- 16. Kim, Jung Taek, and Jeong Joon Yoo. "Implant Design in Cementless Hip Arthroplasty." *Hip & pelvis* 28, no. 2 (2016): 65-75.
- 17. Murthy, P. Balakrishna, A. Sairam Kishore, and P. Surekha. "Acute Toxicological Effects of Multi-Walled Carbon Nanotubes (MWCNT) Nanotechnology and NanomaterialsCarbon Nanotubes-Growth and Applications Edited by Dr." *Mohammad Naraghi* (2011).
- 18. Sivarasu, Sudesh, Pearline Beulah, and Lazar Mathew. "Optimization of skeletal hip implant cross-sections." In *National Conference on Computational Instrumentation-NCCI*, pp. 37-43. 2010.
- 19. Scheerlinck, T., and P-P. Casteleyn. "The design features of cemented femoral hip implants." *Bone & Joint Journal* 88, no. 11 (2006): 1409-1418.
- 20. Singh, Shantanu, and A. P. Harsha. "Analysis of Femoral Components of Cemented Total Hip Arthroplasty." *Journal of The Institution of Engineers (India): Series D* 97, no. 2 (2016): 113-120.
- 21. Zant, Nikolaus P., Charles KY Wong, and Jie Tong. "Fatigue failure in the cement mantle of a simplified acetabular replacement model." *International journal of fatigue* 29, no. 7 (2007): 1245-1252.
- 22. Lewis, Gladius. "Properties of acrylic bone cement: state of the art review." *Journal of Biomedical Materials Research Part A* 38, no. 2 (1997): 155-182.
- 23. Webb, J. C. J., and R. F. Spencer. "The role of polymethylmethacrylate bone cement in modern orthopaedic surgery." *Bone & Joint Journal* 89, no. 7 (2007): 851-857.
- 24. Ledlie, Jon T., and Mark Renfro. "Balloon kyphoplasty: one-year outcomes in vertebral body height restoration, chronic pain, and activity levels." *Journal of Neurosurgery: Spine* 98, no. 1 (2003): 36-42.
- 25. Kühn, Klaus-Dieter. Bone cements: up-to-date comparison of physical and chemical properties of commercial materials. Springer Science & Business Media, 2012.
- 26. Lamb, D. J., Bryan Ellis, and David Priestley. "The effects of process variables on levels of residual monomer in autopolymerizing dental acrylic resin." *Journal of dentistry* 11, no. 1 (1983): 80-88.

- 27. Abouazza, Omar Ali, Finbarr Condon, Ailish Hannigan, and Colum Dunne. "In vitro comparative assessment of the mechanical properties of PMMA cement and a GPC cement for vertebroplasty." *Journal of orthopaedics* 13, no. 2 (2016): 81-89.
- 28. Kim, Seok Bong, Young Jick Kim, Taek Lim Yoon, Su A. Park, In Hee Cho, Eun Jung Kim, In Ae Kim, and Jung-Woog Shin. "The characteristics of a hydroxyapatite–chitosan–PMMA bone cement." *Biomaterials* 25, no. 26 (2004): 5715-5723.
- 29. Goto, Koji, J. Tamura, S. Shinzato, S. Fujibayashi, M. Hashimoto, M. Kawashita, T. Kokubo, and T. Nakamura. "Bioactive bone cements containing nano-sized titania particles for use as bone substitutes." *Biomaterials* 26, no. 33 (2005): 6496-6505.
- 30. Lewis, Gladius. "Properties of nanofiller-loaded poly (methyl methacrylate) bone cement composites for orthopedic applications: a review." *Journal of Biomedical Materials Research Part B: Applied Biomaterials* 105, no. 5 (2017): 1260-1284.
- 31. Ormsby, Ross, Tony McNally, Christina Mitchell, and Nicholas Dunne. "Influence of multiwall carbon nanotube functionality and loading on mechanical properties of PMMA/MWCNT bone cements." *Journal of Materials Science: Materials in Medicine*21, no. 8 (2010): 2287-2292.
- 32. Salamanca, Eisner, Wei-Fang Lee, Chin-Yi Lin, Haw-Ming Huang, Che-Tong Lin, Sheng-Wei Feng, and Wei-Jen Chang. "A novel porcine graft for regeneration of bone defects." *Materials* 8, no. 5 (2015): 2523-2536.
- 33. Heini, P., and U. Berlemann. "Bone substitutes in vertebroplasty." *European Spine Journal* 10 (2001): S205-S213.
- 34. Liu, Zhenzhen, Yong Tang, Ting Kang, Minyu Rao, Kejia Li, Qin Wang, Changyun Quan, Chao Zhang, Qing Jiang, and Huiyong Shen. "Synergistic effect of HA and BMP-2 mimicking peptide on the bioactivity of HA/PMMA bone cement." *Colloids and Surfaces B: Biointerfaces* 131 (2015): 39-46.
- 35. Kjellson, Fred, Torsten Almén, K. E. Tanner, I. D. McCarthy, and Lars Lidgren. "Bone cement X-ray contrast media: A clinically relevant method of measuring their efficacy." *Journal of Biomedical Materials Research Part B: Applied Biomaterials*70, no. 2 (2004): 354-361.
- 36. Florencio-Silva, Rinaldo, Gisela Rodrigues da Silva Sasso, Estela Sasso-Cerri, Manuel Jesus Simões, and Paulo Sérgio Cerri. "Biology of bone tissue: structure, function, and factors that influence bone cells." *BioMed research international* 2015 (2015).
- 37. Datta, H. K., W. F. Ng, J. A. Walker, S. P. Tuck, and S. S. Varanasi. "The cell biology of bone metabolism." *Journal of clinical pathology* 61, no. 5 (2008): 577-587.

- 38. Bonewald, Lynda F. "The amazing osteocyte." *Journal of bone and mineral research* 26, no. 2 (2011): 229-238.
- 39. Jorge, Janaina Habib, Eunice Teresinha Giampaolo, Ana Lúcia Machado, and Carlos Eduardo Vergani. "Cytotoxicity of denture base acrylic resins: a literature review." *The Journal of prosthetic dentistry* 90, no. 2 (2003): 190-193.
- 40. <u>https://basicmedicalkey.com/cell-structure-and-function-2/</u> (Accessed: November 3, 2017)
- 41. Dias, Kamila Kappke. "Safety Assessment of Polymeric Nanoparticle Carriers for Drug Delivery in Human Osteoblasts." PhD diss., 2017.
- 42. Ribeiro, Marta, Fernando J. Monteiro, and Maria P. Ferraz. "Infection of orthopedic implants with emphasis on bacterial adhesion process and techniques used in studying bacterial-material interactions." *Biomatter* 2, no. 4 (2012): 176-194.
- 43. <u>https://www.gems.gov.za/default.aspx?lZnq+PMcXDU2dQt5GXtXrw</u>== (Accessed: November 3, 2017)
- 44. Jung, Woo Kyung, Hye Cheong Koo, Ki Woo Kim, Sook Shin, So Hyun Kim, and Yong Ho Park. "Antibacterial activity and mechanism of action of the silver ion in Staphylococcus aureus and Escherichia coli." *Applied and environmental microbiology* 74, no. 7 (2008): 2171-2178.
- 45. Wu, Shuilin, Zhengyang Weng, Xiangmei Liu, K. W. K. Yeung, and Paul Chu. "Functionalized TiO2 based nanomaterials for biomedical applications." *Advanced Functional Materials* 24, no. 35 (2014): 5464-5481.
- 46. Brammer, Karla S., Seunghan Oh, John O. Gallagher, and Sungho Jin. "Enhanced cellular mobility guided by TiO2 nanotube surfaces." *Nano letters* 8, no. 3 (2008): 786-793.
- 47. Salarian, Mehrnaz. "A New Generation of Polymer/Ceramic Composite Biomaterials for Bone Regeneration." (2014).
- 48. Wang, Yanli, Lulu Yuan, Chenjie Yao, Jie Fang, and Minghong Wu. "Cytotoxicity evaluation of pH-controlled antitumor drug release system of titanium dioxide nanotubes." *Journal of nanoscience and nanotechnology* 15, no. 6 (2015): 4143-4148.
- 49. Fahim, Narges F., and Tohru Sekino. "A novel method for synthesis of titania nanotube powders using rapid breakdown anodization." *Chemistry of Materials* 21, no. 9 (2009): 1967-1979.

- 50. Regonini, Domenico, Chris R. Bowen, Angkhana Jaroenworaluck, and Ron Stevens. "A review of growth mechanism, structure and crystallinity of anodized TiO2 nanotubes." *Materials Science and Engineering: R: Reports*74, no. 12 (2013): 377-406.
- 51. Zhong, Peng, Yulong Liao, Wenxiu Que, Qiaoying Jia, and Tianmin Lei. "Enhanced electron collection in photoanode based on ultrafine TiO2 nanotubes by a rapid anodization process." *Journal of Solid State Electrochemistry* 18, no. 8 (2014): 2087-2098.
- 52. Huang, Shanshan, Wanting Peng, Chengyun Ning, Qing Hu, and Hua Dong. "Nanostructure transition on anodic titanium: structure control via a competition strategy between electrochemical oxidation and chemical etching." *The Journal of Physical Chemistry C* 116, no. 42 (2012): 22359-22364.
- 53. Ng, S. W., F. K. Yam, K. P. Beh, and Z. Hassan. "Titanium dioxide nanotubes in chloride based electrolyte: an alternative to fluoride based electrolyte." *Sains Malaysiana* 43, no. 6 (2014): 947-951.
- 54. Hahn, R., J. M. Macak, and P. Schmuki. "Rapid anodic growth of TiO 2 and WO 3 nanotubes in fluoride free electrolytes." *Electrochemistry Communications* 9, no. 5 (2007): 947-952.
- 55. Cheong, Y. L., F. K. Yam, S. W. Ng, Z. Hassan, S. S. Ng, and I. M. Low. "Fabrication of titanium dioxide nanotubes in fluoride-free electrolyte via rapid breakdown anodization." *Journal of Porous Materials* 22, no. 6 (2015): 1437-1444.
- Panaitescu, E., C. Richter, and L. Menon. "A study of titania nanotube synthesis in chloride-ion-containing media." *Journal of The Electrochemical Society* 155, no. 1 (2008): E7-E13.
- 57. Hazzazi, Omar Abdullah. "On the pitting corrosion behaviour of pure Al by halide ions in neutral sulphate solutions and the effect of some inorganic inhibitors." *Science* 19, no. 1 (2007).
- 58. Raja, V. S., and Tetsuo Shoji, eds. *Stress corrosion cracking: theory and practice*. Elsevier, 2011.
- 59. Soltis, J. "Passivity breakdown, pit initiation and propagation of pits in metallic materials– review." *Corrosion Science* 90 (2015): 5-22.
- 60. Tsuchiya, Hiroaki, Jan M. Macak, Andrei Ghicov, Luciano Taveira, and Patrik Schmuki. "Self-organized porous TiO 2 and ZrO 2 produced by anodization." *Corrosion Science* 47, no. 12 (2005): 3324-3335.
- 61. Tian, Tian, Xiu-feng Xiao, Rong-fang Liu, and Xiao-feng Hu. "Study on titania nanotube arrays prepared by titanium anodization in NH4F/H2SO4 solution." *Journal of materials science* 42, no. 14 (2007): 5539-5543.

- 62. Smith, York R., Rupashree S. Ray, Krista Carlson, Biplab Sarma, and Mano Misra. "Selfordered titanium dioxide nanotube arrays: anodic synthesis and their photo/electrocatalytic applications." *Materials* 6, no. 7 (2013): 2892-2957.
- 63. Crawford, G. A., and Nikhilesh Chawla. "Porous hierarchical TiO 2 nanostructures: processing and microstructure relationships." *Acta Materialia* 57, no. 3 (2009): 854-867.
- 64. Joseph, S., T. Manovah David, C. Ramesh, and P. Sagayaraj. "The role of electrolyte pH in enhancing the surface morphology of TiO2 nanotube arrays grown on Ti Substrate." *IJSER* 5 (2014): 85-91.
- Antony, Rajini P., Tom Mathews, Arup Dasgupta, S. Dash, A. K. Tyagi, and Baldev Raj. "Rapid breakdown anodization technique for the synthesis of high aspect ratio and high surface area anatase TiO 2 nanotube powders." *Journal of Solid State Chemistry* 184, no. 3 (2011): 624-632.
- 66. Chen, Jingfei, Jia Lin, and Xianfeng Chen. "Self-assembled TiO 2 nanotube arrays with Ushaped profile by controlling anodization temperature." *Journal of Nanomaterials* 2010 (2010): 38.
- 67. Indira, K., U. Kamachi Mudali, T. Nishimura, and N. Rajendran. "A review on TiO2 nanotubes: influence of anodization parameters, formation mechanism, properties, corrosion behavior, and biomedical applications." *Journal of Bio-and Tribo-Corrosion* 1, no. 4 (2015): 28.
- 68. Allam, Nageh K., and Craig A. Grimes. "Effect of cathode material on the morphology and photoelectrochemical properties of vertically oriented TiO 2 nanotube arrays." *Solar Energy Materials and Solar Cells* 92, no. 11 (2008): 1468-1475.
- 69. Yun, Sining, Yanfang Liu, Taihong Zhang, and Shahzada Ahmad. "Recent advances in alternative counter electrode materials for Co-mediated dye-sensitized solar cells." *Nanoscale* 7, no. 28 (2015): 11877-11893.
- 70. Bard, A. J., L. R. Faulkner, E. Swain, and C. Robey. "Electrochem. Meth. Fundamentals Applications." (1980).
- 71. Oldham, Keith, Jan Myland, and Alan Bond. *Electrochemical science and technology: fundamentals and applications*. John Wiley & Sons, 2011.
- 72. Mor, Gopal K., Oomman K. Varghese, Maggie Paulose, Karthik Shankar, and Craig A. Grimes. "A review on highly ordered, vertically oriented TiO 2 nanotube arrays: fabrication, material properties, and solar energy applications." *Solar Energy Materials and Solar Cells* 90, no. 14 (2006): 2011-2075.

- 73. Sato, N., K. Kudo, and T. Noda. "The anodic oxide film on iron in neutral solution." *Electrochimica Acta* 16, no. 11 (1971): 1909-1921.
- 74. Sato, Norio. "A theory for breakdown of anodic oxide films on metals." *Electrochimica Acta* 16, no. 10 (1971): 1683-1692.
- 75. Macak, Jan M., K. Sirotna, and P. Schmuki. "Self-organized porous titanium oxide prepared in Na 2 SO 4/NaF electrolytes." *Electrochimica Acta* 50, no. 18 (2005): 3679-3684.
- 76. Albu, Sergiu P., Poulomi Roy, Sannakaisa Virtanen, and Patrik Schmuki. "Self-organized TiO2 Nanotube Arrays: Critical Effects on Morphology and Growth." *Israel Journal of Chemistry* 50, no. 4 (2010): 453-467.
- 77. Patel, Sweetu, Giovanni Francesco Solitro, Cortino Sukotjo, Christos Takoudis, Mathew T. Mathew, Farid Amirouche, and Tolou Shokuhfar. "Nanotopography and surface stress analysis of Ti6Al4V bioimplant: an alternative design for stability." *JOM* 67, no. 11 (2015): 2518-2533.
- 78. Kapusta-Kołodziej, Joanna, Olena Tynkevych, Anna Pawlik, Magdalena Jarosz, Justyna Mech, and Grzegorz D. Sulka. "Electrochemical growth of porous titanium dioxide in a glycerol-based electrolyte at different temperatures." *Electrochimica Acta* 144 (2014): 127-135.
- 79. Kasuga, Tomoko, Masayoshi Hiramatsu, Akihiko Hoson, Toru Sekino, and Koichi Niihara. "Titania nanotubes prepared by chemical processing." *Advanced Materials* 11, no. 15 (1999): 1307-1311.
- 80. Li, Jianlin, Qingliu Wu, and Ji Wu. "Synthesis of Nanoparticles via Solvothermal and Hydrothermal Methods." *Handbook of Nanoparticles* (2016): 295-328.
- 81. Ou, Hsin-Hung, and Shang-Lien Lo. "Review of titania nanotubes synthesized via the hydrothermal treatment: fabrication, modification, and application." *Separation and Purification Technology* 58, no. 1 (2007): 179-191.
- 82. Aliofkhazraei, Mahmood. *Handbook of Functional Nanomaterials*. *Volume 4-Properties and Commercialization*. Nova Science Publishers Incorporated, 2014.
- 83. Walton, Richard I. "Subcritical solvothermal synthesis of condensed inorganic materials." *Chemical Society Reviews* 31, no. 4 (2002): 230-238.
- 84. Einarsrud, Mari-Ann, and Tor Grande. "1D oxide nanostructures from chemical solutions." *Chemical Society Reviews* 43, no. 7 (2014): 2187-2199.

- 85. Rabenau, Albrecht: "The role of hydrothermal synthesis in preparative chemistry." *Angewandte Chemie International Edition* 24, no. 12 (1985): 1026-1040.
- Sheets, William C., Emmanuelle Mugnier, Antoine Barnabé, Tobin J. Marks, and Kenneth R. Poeppelmeier. "Hydrothermal synthesis of delafossite-type oxides." *Chemistry of materials*18, no. 1 (2006): 7-20.
- 87. Gupta, Shipra, and Manoj Tripathi: "A review on the synthesis of TiO2 nanoparticles by solution route." *Open Chemistry* 10, no. 2 (2012): 279-294.
- 88. Jouyban, Abolghasem, Shahla Soltanpour, and Hak-Kim Chan. "A simple relationship between dielectric constant of mixed solvents with solvent composition and temperature." *International journal of pharmaceutics* 269, no. 2 (2004): 353-360.
- 89. Akerlof, G. C., and H. I. Oshry. "The dielectric constant of water at high temperatures and in equilibrium with its vapor." *Journal of the American Chemical Society* 72, no. 7 (1950): 2844-2847.
- 90. Abdullah, Masturah, and Siti Kartom Kamarudin. "Pengaruh kepekatan sodium hidrosida (NaOH) yang tinggi terhadap pembentukan struktur bertertib nanotiub TiO2 (TNT)." *Malaysian Journal of Analytical Sciences* 20, no. 6 (2016): 1405-1412.
- 91. Liu, Nan, Xiaoyin Chen, Jinli Zhang, and Johannes W. Schwank. "A review on TiO 2based nanotubes synthesized via hydrothermal method: formation mechanism, structure modification, and photocatalytic applications." *Catalysis Today*225 (2014): 34-51.
- 92. Sreekantan, Srimala, and Lai Chin Wei. "Study on the formation and photocatalytic activity of titanate nanotubes synthesized via hydrothermal method." *Journal of Alloys and Compounds* 490, no. 1 (2010): 436-442.
- 93. Bavykin, Dmitry V., Valentin N. Parmon, Alexei A. Lapkin, and Frank C. Walsh. "The effect of hydrothermal conditions on the mesoporous structure of TiO 2 nanotubes." *Journal of Materials Chemistry* 14, no. 22 (2004): 3370-3377.
- 94. Vu, Thu Ha Thi, Hang Thi Au, Lien Thi Tran, Tuyet Mai Thi Nguyen, Thanh Thuy Thi Tran, Minh Tu Pham, Manh Hung Do, and Dinh Lam Nguyen. "Synthesis of titanium dioxide nanotubes via one-step dynamic hydrothermal process." *Journal of Materials Science* 49, no. 16 (2014): 5617-5625.
- 95. Nakahira, Atsushi, Takashi Kubo, and Chiya Numako. "Formation mechanism of TiO2derived titanate nanotubes prepared by the hydrothermal process." *Inorganic chemistry*49, no. 13 (2010): 5845-5852.

- 96. Wong, Chung Leng, Yong Nian Tan, and Abdul Rahman Mohamed. "A review on the formation of titania nanotube photocatalysts by hydrothermal treatment." *Journal of environmental management* 92, no. 7 (2011): 1669-1680.
- 97. Yuan, Zhong-Yong, and Bao-Lian Su. "Titanium oxide nanotubes, nanofibers and nanowires." *Colloids and Surfaces A: Physicochemical and Engineering Aspects* 241, no. 1 (2004): 173-183.
- 98. Poudel, B., W. Z. Wang, C. Dames, J. Y. Huang, S. Kunwar, D. Z. Wang, D. Banerjee, G. Chen, and Z. F. Ren. "Formation of crystallized titania nanotubes and their transformation into nanowires." *Nanotechnology* 16, no. 9 (2005): 1935.
- 99. Tsai, Chien-Cheng, and Hsisheng Teng. "Regulation of the physical characteristics of titania nanotube aggregates synthesized from hydrothermal treatment." *Chemistry of Materials* 16, no. 22 (2004): 4352-4358.
- 100. Mozia, Sylwia, Ewa Borowiak-Paleń, Jacek Przepiórski, Barbara Grzmil, Tomoki Tsumura, Masahiro Toyoda, Joanna Grzechulska-Damszel, and Antoni W. Morawski. "Physico-chemical properties and possible photocatalytic applications of titanate nanotubes synthesized via hydrothermal method." *Journal of Physics and Chemistry of Solids* 71, no. 3 (2010): 263-272.
- 101. Jiang, Fang, Shourong Zheng, Lichao An, and Huan Chen. "Effect of calcination temperature on the adsorption and photocatalytic activity of hydrothermally synthesized TiO 2 nanotubes." *Applied Surface Science* 258, no. 18 (2012): 7188-7194.
- 102. Qi, Mei-Li, Kun He, Zhen-Nan Huang, Reza Shahbazian-Yassar, Gui-Yong Xiao, Yu-Peng Lu, and Tolou Shokuhfar. "Hydroxyapatite Fibers: A Review of Synthesis Methods." JOM 69, no. 8 (2017): 1354-1360.
- 103. Agrawal, Megha, Vivek Kumar, Abhishek K. Singh, Mahendra P. Kashyap, Vinay K. Khanna, Maqsood A. Siddiqui, and Aditya B. Pant. "trans-Resveratrol protects ischemic PC12 Cells by inhibiting the hypoxia associated transcription factors and increasing the levels of antioxidant defense enzymes." ACS chemical neuroscience 4, no. 2 (2012): 285-294.
- 104. Geng, Zhen, Zhenduo Cui, Zhaoyang Li, Shengli Zhu, Yanqin Liang, Yunde Liu, Xue Li et al. "Strontium incorporation to optimize the antibacterial and biological characteristics of silver-substituted hydroxyapatite coating." *Materials Science and Engineering: C* 58 (2016): 467-477.
- 105. Suzuki, Yoshikazu, and Susumu Yoshikawa. "Synthesis and thermal analyses of TiO 2derived nanotubes prepared by the hydrothermal method." *Journal of Materials Research* 19, no. 4 (2004): 982-985.

- 106. Mousa, Weam F., Masahiko Kobayashi, Shuichi Shinzato, Masaki Kamimura, Masashi Neo, Satoru Yoshihara, and Takashi Nakamura. "Biological and mechanical properties of PMMA-based bioactive bone cements." *Biomaterials* 21, no. 21 (2000): 2137-2146.
- 107. P. Population and P. M. Review, "Total Knee Replacement," *Physiotherapy*, no. April, pp. 0–39, 2009.
- 108. Saleh, Khaled J., Mouhanad M. El Othmani, Tony H. Tzeng, William M. Mihalko, Monique C. Chambers, and Thomas M. Grupp. "Acrylic bone cement in total joint arthroplasty: A review." Journal of Orthopaedic Research 34, no. 5 (2016): 737-744.

VITA

NAME:	Abhijit Haribhau Phakatkar	
EDUCATION:	University of Illinois at Chicago, IL Master of Science in Mechanical Engineering, 2017	
	University of Pune, India Degree: Bachelor of Technology in Mechanical Engineering, 2012	
EXPERIENCE:	In-situ Nanomedicine Laboratory (ISNL), Chicago, USA University of Illinois at Chicago (January 2016- present) Research Assistant	
	Automotive Research Association of India (ARAI), Pune, India (March 2015 - July 2015) Internship trainee	
	Vishwakarma Institute of Technology, Pune, India (December 2014 – February 2015) Research Assistant	
	Mahindra & Mahindra Ltd., Nasik, India (October 2012 - April 2014) Assistant Manager	
	Supra SAE India (F1 vehicle competition), Delhi, India (August 2011 & September 2012)	